博士論文

Identification of EPSIN3 and CYSTATIN C as novel p53-inducible targets and their functional analysis

(*p53*新規下流標的としてのエプシン3, シスタチンCの同定および機能解析)

森　甚一

Contents

Abstract

p53 is one of the most intensively studied tumor suppressor genes. Recent cancer genomic analyses using next-generation sequencing technique revealed that mutations of the *p53* gene are still the most common alteration observed in the majority of human cancers. Alterations in the *p53* gene are clustered in its DNA-binding domain, implying that transactivation of target genes is pivotal mechanism of tumor suppressive function of p53, and therefore identification and functional analysis of p53-targets are of importance in cancer research. A number of p53 target genes have been previously isolated. However, the full picture of the p53 downstream pathway still remains to be elucidated. To identify novel p53 targets, we here performed transcriptome and proteome analysis, and I further analyzed the function of the newly identified genes.

To identify novel p53 targets, we conducted cDNA microarray analysis and mass spectrometry analysis using mRNAs and whole cell lysates, respectively, isolated from HCT116*p53*$^{+/+}$ and HCT116 *p53*$^{-/-}$ cells that were treated with 2 μg/ml of ADR. RNA and protein were collected at 0, 12, 24, 48, and 72 h after ADR treatment. We obtained expression data of total 22,275 genes from the transcriptome analysis and 3,363 proteins from the proteome analysis. After applying the screening criteria, I identified 166 genes and 91 proteins including 16 and 6 known p53-downstream targets, respectively. Among the novel candidates, I selected *EPSIN3* from transcriptome analysis and CYSTATIN C from proteome analysis. To confirm the result of cDNA microarray and mass spectrometry analysis, I performed qPCR analysis and western blot analysis. I found that EPSIN3 and CYSTATIN C were remarkably induced by ADR in a p53-dependent manner. Next, I surveyed for p53 binding sequence (p53BS) within their genetic loci and identified two p53BSs in the promoter region of the *EPSIN3* gene and one p53BS in the first intron in the *CYSTATIN C* gene. The DNA fragments containing p53BSs were amplified and subcloned upstream of the minimal promoter in pGL4.24 vector (pGL4.24/p53BS). The result of reporter assay revealed that U373MG cells transfected with pGL4.24/p53BS showed

increased luciferase activity only in the presence of plasmid expressing wild-type p53. To verify whether p53 could directly bind to p53BSs, I performed ChIP assay using U373MG cells that were infected with either Ad-p53 or Ad-LacZ. After precipitation by an anti-p53 antibody, DNA fragments harboring BSs were quantified by qPCR. As a result, p53 specifically bound to p53BS2 (*EPSIN3*) and p53BS (*CYSTATIN C*) in cells infected with Ad-p53.

Epsins are accessory proteins implicated in clathrin-mediated endocytosis by binding ubiquitin moieties on the cytoplasmic part of membrane proteins. To date, the functions of EPSIN3 in both normal and cancer cells are largely unknown. To explore the role of EPSIN3 in the growth of cancer cells, I performed colony formation assay using three cancer cell lines: H1299, HCT116, and U373MG. As a result, colony formation was significantly impaired in HCT116 and U373MG cells which had been transfected with EPSIN3 expressing plasmid compared with mock. I subsequently analyzed cell viability by ATP measurement assay and found that EPSIN3 knockdown inhibited the ADR-induced growth suppression to the same degree as cells treated with sip53. I further examined the impact of EPSIN3 on ADR-induced apoptosis. Interestingly, knockdown of EPSIN3 in ADR-treated HCT116 cells increased pro-caspase 3 and reduced cleaved caspase3, indicating the regulation of apoptosis by EPSIN3.

Cystatins are reversible, tight binding inhibitors against C1 cysteine proteases, which exert various physiological functions. Among the family, CYSTATIN C has been the most intensively studied and shown to inhibits cathepsin L, a lysosomal cysteine protease, that is highly expressed in various cancer cells and is involved in cancer development and progression. First, I analyzed cell viability by ATP measure assay and found that CYSTATIN C knockdown inhibited the ADR-induced growth suppression to the same degree as cells treated with sip53. Next, I found that knockdown of CYSTATIN C in ADR-treated HCT116 cells increased pro-caspase 3 and reduced cleaved caspase 3, indicating the regulation of apoptosis by CYSTATIN C. When HEK293T cells were transfected with

plasmid expressing CYSTATIN C, cathepsin L activity was markedly decreased compared with mock-transfected cells. Then I measured cathepsin L activity in HCT116 *p53*$^{-/-}$, *p53*$^{+/+}$ or CYSTATIN C-silenced *p53*$^{+/+}$ cells that were treated with ADR. As a result, cathepsin L activity was significantly reduced in HCT116 *p53*$^{+/+}$ cells after ADR treatment, while ADR treatment increased cathepsin L activity in *p53*$^{-/-}$ cells or CYSTATIN C-silenced *p53*$^{+/+}$ cells. These results indicated that p53-CYSTATIN C pathway regulates cathepsin L activity.

I identified EPSIN3 and CYSTATIN C as novel p53 targets using transcriptome and proteome analysis, respectively. Both genes promote apoptosis of cancer cells in regulation of p53.

Introduction

p53 is one of the most intensively studied tumor suppressor genes [1-3]. p53 is a short-lived transcription factor and its intracellular level is maintained to be low through proteasomal degradation, which is mainly mediated by E3 ligase activity of murine double minute 2 (MDM2) [4, 5]. p53 transactivates MDM2 expression through the promoters of MDM gene and constitutes a negative feedback loop, resulting in maintaining itself at appropriate level (Figure 1). When cells are exposed to cellular stresses such as DNA damage, hypoxia, or oncogene activation, ataxia telangiectasia mutated (ATM) are activated. ATM inhibits E3 ligase functions of MDM2 through phosphorylation of the catalytic domain of MDM2, and subsequently prevents p53 from ubiquitin-proteasomal degradation [6] (Figure 2). Moreover, a number of modifications within p53 itself simultaneously occur. Within 30 min after DNA damage, Ser^{15} of p53 is phosphorylated by ATM followed by subsequent phosphorylation of Thr^{18} by CK1 and Ser^{20} by CHK2 [7-9]. These modifications negatively affect the p53-MDM2 interaction, resulting in p53 stabilization.

Thus, p53 activated by cellular stresses induces transcription of hundreds of its target genes and exerts various functions such as cell cycle arrest, senescence, apoptosis, and posttranscriptional modification [10-12] (Figure 3). Mutations of p53 gene has been found in approximately 50% of human cancers [13], and recent cancer genomic analyses using next-generation sequencing technique further revealed that mutations of the *p53* gene are still the most common alteration observed in the majority of human cancers [14]. According to International Agency for Research on Cancer TP53 database, 73% of alterations in p53 gene are missense mutations and 98% of those are clustered in its DNA-binding domain through which the p53 protein binds to specific DNA element [15, 16]. Kato and co-workers examined transcriptional activities of 2,314 missense mutant-p53 using site-directed mutagenesis and showed that 64% of mutations in the

DNA-binding domain of p53 result in loss of its transcriptional activity [17]. These observations imply that transactivation of target genes is pivotal mechanism of tumor suppressive function of p53, and therefore identification and functional analysis of p53-targets are of importance in cancer research. Our group have previously identified a number of p53-target genes. In 2000, using a yeast enhancer trap system [18], I screened human genomic sequences which activates transcription in p53-dependent manner, and isolated *p53AIP1* as a novel p53-target gene involved in apoptosis [19]. In the same year, using differential display method [20], we isolated *p53R2*, which plays a role in DNA repair under the regulation of *p53* [21]. To comprehensively screen p53-targets, we performed cDNA microarray using U373MG cells (glioblastoma with *p53* mutation) infected with adenovirus designed to express p53 [22] and identified *p53RDL1* as an effecter of p53-mediated apoptosis. Using the same method, we subsequently identified three novel p53-targets: *XEDAR*, *PADI4, and ISCU,* which are involved in anoikis, histone modification, and iron regulation, respectively [12, 23-25]. In spite of the researchers' efforts, full picture of the p53 downstream pathway still remains to be elucidated and recent exhaustive methods have suggested that numerous unknown targets exist. To identify novel p53-targets, we here performed transcriptome and proteome analysis and further analyzed the function of novel p53 targets.

Materials and Methods

cDNA microarray

Gene expression analysis was performed using SurePrint G3 Human GE 8 × 60K microarray (Agilent, Santa Clara, CA, USA) according to the manufacturer's protocol. Briefly, HCT116 $p53^{+/+}$ or HCT116 $p53^{-/-}$ cells were treated with ADR and incubated at 37°C until the time of harvest. Total RNA was isolated from the cells using standard protocols. Each RNA sample was labeled and hybridized to array slides.

Mass spectrometric analysis.

Cells were lysed in [8M urea, 50 mM HEPES-NaOH, pH = 8.0] and reduced with 10 mM tris(2-carboxyethyl)phosphine (Sigma-Aldrich, St. Louis, MO, USA)) at 37°C for 30 min, followed by alkylation with 50 mM iodoacetamide (Sigma-Aldrich) at 25°C in dark for 45 min. Proteins were digested with Immobilized trypsin (Thermo Scientific, Waltham, MA, USA) at 37°C for 6 hours. The resulting peptides were desalted by Oasis HLB μ-elution plate (Waters , Milford, MA, USA) and analyzed by LTQ-Orbitrap-Velos mass spectrometer (Thermo Scientific) combined with UltiMate 3000 RSLC nano-flow HPLC system (Thermo Scientific). The MS/MS spectra were searched against *Homo sapiens* protein sequence database in SwissProt using Proteome Discoverer 1.4 software (Thermo Scientific), in which false discovery rate of 1% was set for both peptide and protein identification filters. Differential peptide quantification analysis (label-free quantification analysis) for 10 samples was performed on Expressionist Server platform (Genedata AG, Swiss) as described previously [26].

Cell culture and transfection.

Human embryonic kidney cells HEK293T were obtained from Riken Cell Bank (Ibaraki, Japan). Human cancer cell lines U373MG (astrocytoma), H1299 (non-small cell lung

cancer), HCT116 (colorectal adenocarcinoma), and HBL100 (breast carcinoma) were purchased from American Type Culture Collection. Huma n mammary epithelial cells MCF10A *p53*$^{+/+}$ or MCF10A *p53*$^{-/-}$ were purchased from Sigma Aldrich. HBC4 (breast carcinoma) was gifted from T. Yamori (Japanese Foundation for Cancer Research, Tokyo, Japan). HCT116 *p53*$^{+/+}$ and HCT116 *p53*$^{-/-}$ cell lines were gifts from B. Vogelstein (Johns Hopkins University, Baltimore, MD, USA). HEK293T and U373MG cells were transfected with plasmids using Fugene6 (Promega, Madison, WI, USA), and Lipofectamin LTX (Invitrogen, Carlsbad, CA, USA), respectively. Small interfering RNA (siRNA) oligonucleotides, commercially synthesized by Sigma Genosys (Woollands, TX, USA), were transfected with Lipofectamine RNAiMAX reagent (Invitrogen). Sequences of siRNA oligonucleotides are shown in Table 1.

Cell treatments

We generated and purified replication-deficient recombinant viruses expressing p53 (Ad-p53) or LacZ (Ad-LacZ) as described previously [19]. U373MG (*p53*-mutant) and H1299 (*p53*-deficient) cells were infected with viral solutions at various amounts of multiplicity of infection (MOI) and incubated at 37°C until the time of harvest. For treatment with genotoxic stress, cells were incubated with 2 μg/ml of adriamycin (ADR) for 2 h. As oxidative stress, cells were continuously incubated in medium with 200mM Hydrogen peroxide (H_2O_2) (Wako, Osaka, Japan) at 37°C until the time of harvest.

Quantitative real-time PCR.

Total RNA was isolated from human cells and mouse tissues using RNeasy Plus Mini Kits (Qiagen, Valencia, CA, USA) according to the manufacturer's instructions. Complementary DNAs were synthesized using Super Script III reverse transcriptase (Invitrogen). Quantitative real-timePCR (qPCR) was conducted using SYBR Green

Master Mix on a Light Cycler 480 (Roche, Basel, Switzerland). Primer sequences are shown in Table 1.

Western blot analysis

To prepare whole cell extracts, cells were collected and lysed in chilled RIPA buffer (50 mmol/L Tris-HCl at pH 8.0, 150 mmol/L NaCl, 0.1% SDS, 0.5% sodium deoxycholate, and 1% NP40) containing 1 mM phenyl methylsulphonyl fluoride (PMSF), 0.1 mM DTT and 0.1% Calbiochem Protease Inhibitor Cocktail Set III, EDTA-Free (EMD Chemicals Inc., Merck KGaA, Darmstadt, Germany). Samples were sonicated for 15 min with a 30-sec on/30-sec off cycle using Bioruptor UCD-200 (Cosmobio, Tokyo, Japan). After centrifugation at 16,000 × *g* for 15 min, supernatants were collected and boiled in SDS sample buffer (Biorad, Hercules, CA, USA). SDS-polyacrylamide gel electrophoresis (SDS-PAGE) was performed for each sample, and the proteins were then transferred to a nitrocellulose membrane (Hybond™ ECL™, Amersham, Piscataway, NJ, USA). Protein bands on western blots were visualized by ECL Western Blotting Detection Reagent (Amersham) or Immnobilon Western Chemiluminescent HRP Substrate (Merck Millipore, Darmstadt, Germany).

Antibodies

Anti-actin monoclonal antibody (AC15) and anti-EPSIN3 polyclonal antibody (HPA055546) were purchased from Sigma-Aldrich. Anti- CYSTATIN C monoclonal antibody (C27) was purchased from Santa Cruz Biotechnology (Santa Cruz, CA, USA). Anti-p21 monoclonal antibody (OP64) and anti-p53 monoclonal antibody (OP43) were purchased from Merck Millipore. Anti-caspase 3 monoclonal antibody (8G10) and anti-cleaved caspase 3 monoclonal antibody (5A1E) were purchased from Cell Signaling Technology (Beverly, MA, USA).

Gene reporter assay

DNA fragments, including the potential p53-binding sequence were amplified and subcloned into the pGL4.24-promoter vector (Promega). Primers for amplification are shown in Table 1. Point mutations "T" were inserted at the 4th and the 14th nucleotide "C" and the 7th and the 17th nucleotide "G" of the potential p53-binding sequence by site-directed mutagenesis (Table 1). Reporter assays were performed using the Dual Luciferase assay system (Promega) as described previously [23].

Chromatin immunoprecipitation assay.

ChIP assay was performed using EZ-Magna ChIP G Chromatin Immunoprecipitation Kit (Merck Millipore) following the manufacturer's protocol. In brief, U373MG cells infected with Ad-p53 or Ad-LacZ at an MOI of 10 were cross-linked with 1% formaldehyde for 10 min, washed with PBS, and lysed in nuclear lysis buffer. The lysate was then sonicated using Bioruptor UCD-200 (CosmoBio) to shear DNA to approximately 200-1000 bp. Supernatant from 1×10^6 cells was used for each immunoprecipitation with anti-p53 antibody (OP140, Merck Millipore) or normal mouse IgG (sc-2025, Santa Cruz). Before immunoprecipitation, 2% of supernatant was removed as "input". Column-purified DNA was quantified by qPCR. Primer sequences are shown in Table 1.

Cell proliferation and apoptosis analysis

HCT116 cells were seeded on cell-culture dishes coated with polyethyleneimine and transfected with siRNAs. At 24 h after transfection, cells were transfered to ultra-low attachment plates (Corning, NY, USA). After another 24 h, cells were treated with 1 μg/ml of ADR for 48 h. To assess cell viability, cells were subjected to ATP measurement

assay using Cell Titer-Glo Luminescent Viability Assay (Promega) according to the manufacturer's protocol. For the detection of apoptosis, cells treated as above were subjected to western blot analysis by using anti-pro-caspase 3 and cleaved caspase 3 antibodies.

Plasmid construction.

The entire coding sequences of *EPSIN 3* and *CYSTATIN C* cDNA were amplified by PCR using KOD-Plus DNA polymerase (Toyobo, Osaka, Japan), and inserted into the *Eco*RI and *Xho*I sites of pCAGGS vector. The constructs were confirmed by DNA sequence analysis. Primers used for amplification are shown in Table 1.

Immunocytochemistry

Adherent cells were fixed with 4% paraformaldehyde in PBS and permeabilized with 0.2% Triton X-100 in PBS for 5 min at room temperature. The cells were then covered with blocking solution (3% BSA/PBS containing 0.2% Triton X-100) for 1 h at room temperature and incubated with rabbit anti-EPSIN 3 antibody (diluted 1:500) or mouse anti-p53 antibody (diluted 1:1000) in blocking solution overnight at 4 °C. Primary antibodies were stained with goat anti-rabbit or anti-mouse secondary antibodies conjugated to Alexa488 or Alexa594 (each diluted 1:2000) for 1h at room temperature, stained with DAPI and visualized with Fluoview FV1000 confocal microscope (Olympus, Tokyo, Japan).

Knockout mouse

p53-deficient mice were provided from RIKEN BioResource Center (Ibaraki, Japan) [27]. Genotypes were confirmed by PCR analysis. Frozen sperms of *Epsin 3*$^{/+}$ C57BL/6N mice were purchase from UC Davis Knockout Mouse Depository (vector design is shown in

Figure 23). After *Epsin 3*$^{+/+}$ mice were obtained by *in vitro* fertilization, *Epsin 3*$^{-/-}$ mice were generated from male/female pairs of *Epsin 3*$^{+/+}$ mice. The primer sequences are indicated in Table 1. All mice were maintained under specific pathogen-free conditions and were handled in accordance with the Guidelines for Animal Experiments of the Institute of Medical Science (University of Tokyo, Tokyo, Japan).

Immnohistochemistry

Sections of stomach of 6-week-old mice that were formalin-fixed and paraffin-embedded were subjected to immunohistochemistry. After deparaffinization with xylene, antigen was retrieved at 125°C for 30sec in DAKO Target Retrieval Solution (EDTA buffer, pH 6.0). Intrinsic peroxidase and proteins were blocked. Anti- Epsin 3 antibody diluted to 1/150 with DAKO Antibody Diluent was added to the samples and incubated for 1 h at 37^{0}C and subsequently reacted with Envision Plus anti-rabbit IgG as a 2nd antibody for 1 h at 37^{0}C. Substrate chromogen was added, and the specimens were counterstained with haematoxylin.

Wound healing experiment

A Full-thickness excisional wounds were created on the dorsum of Six-week-old *Epsin 3*$^{-/-}$ *or Epsin 3*$^{+/+}$ *mice* using a 5 mm diameter of biopsy punch (Kai Medical, Gifu, Japan). The wounds were photographed at day 0, 3, 5 and 7 and the area of wounds were calculated by Adobe PhotoShop CS3 (Adobe Systems, San Jose, USA)

Survival and tumor development assay

For survival analysis, 8 *Epsin 3*$^{-/-}$ and *14 Epsin 3*$^{+/+}$ mice at the age of 6 weeks were irradiated with 10 Gy of X-ray using X-ray irradiation system (MBR-1520R-3,Hitachi). Overall survival was defined as the days from irradiation to death from any cause. To

initiate tumor development, 19 *Epsin 3*$^{-/-}$ and 14 *Epsin 3*$^{+/+}$ mice at the age of 6 weeks were irradiated with 4 Gy of X-ray at day 1, 8, 15, and 21. Tumor-free survival was defined as the days from irradiation to appearance of tumor or death from any cause.

Cathepsin L activity assay

Cathepsin L activity assay was performed using Cathepsin L Activity Assay Kit (Promokine, Heidelberg, Germany) following the manufacturer's protocol. Briefly, HEK 293T cells transfected with CYSTATIN C expression plasmid or mock plasmid were collected at 36 h after transfection. HCT116 *p53*$^{-/-}$, HCT116 *p53*$^{+/+}$, or CYSTATIN C-silenced HCT116 *p53*$^{+/+}$ cells treated with 2 μg/ml of ADR for 2 h were collected 48 h after treatment. The cells were lysed with lysis buffer provided in the kit. Protein concentration of each lysate was measured by Pierce BCA Protein Asssay Kit (Thermo Fisher Scientific) and diluted to 0.60 μg/μl. After adding DTT for a final concentration of 4 mM and fluorescent substrate to the lysates, samples were incubated for 1 h at 37°C, and fluorescence was measured at ex 405 / em 500 in ARVO X3 plate reader (Perkin Elmer).

Database analysis

EPSIN 3 and CYSTATIN C expression level in clinical samples were obtained from the TCGA project via data portal on 15 May 2015 [28]. *p53* mutation status in cancer tissues were collected from the TCGA website, and the expression levels of *CYSTATIN C in* three sample categories: normal tissues, tumors with wild-type p53, and tumors with mutant p53 were compared using the Mann-Whitney U test. Clinical data was also downloaded from the TCGA website and survival analysis was performed using log-rank test stratified by expression level of *CYSTATIN C* in tumor (above or below the median expression level of the cohort).

Results

Screening of p53 downstream targets

To identify novel p53-targets, we conducted cDNA microarray analysis and mass spectrometry analysis using mRNAs and whole cell lysates, respectively, isolated from HCT116*p53*$^{+/+}$ and HCT116 *p53*$^{-/-}$ cells that were treated with 2 μg/ml of ADR (Figure 3). RNA and protein were collected at 0, 12, 24, and 48 (protein was additionally collected at 72 h), after ADR treatment. Gene expression analysis was performed using SurePrint G3 Human GE 8 × 60K microarray. Protein expression was determined by LC-MS/MS analysis. We obtained expression data of total 22,275 genes from the transcriptome analysis and 3,363 proteins from the proteome analysis. To screen candidates that were induced by ADR damage in p53-dependent manner, I applied the following criteria;

1) The intensity in HCT116 *p53*$^{+/+}$ cells is 10-fold higher in transcriptome analysis and 3-fold higher in proteome analysis than that in HCT116 *p53*$^{-/-}$ cells at 2 or more time points,
2) In HCT116 *p53*$^{+/+}$ cells, the intensities are 3-fold higher than that at 0 hours at 2 or more time points,
3) The maximum intensity in HCT116 *p53*$^{+/+}$ cells is 2-fold higher than that in HCT116 *p53*$^{-/-}$ cells

After this screening, I identified 166 genes and 91 proteins including 16 and 6 known p53-downstream targets, respectively. Among the novel candidates, I selected *EPSIN 3* (*EPN3*) from transcriptome analysis and CYSTATIN C (*CST3*) from proteome analysis because they were markedly induced.

EPSIN 3 and CYSTATIN C are induced by DNA damage and p53

To confirm the result of cDNA microarray and mass spectrometry analysis, I performed

quantitative real-time PCR (qPCR) analysis. I found that *EPSIN 3* and *CYSTATIN C* mRNA were remarkably induced by ADR only in HCT116 $p53^{+/+}$ cells (Figure 4, 8). In accordance with the qPCR results, EPSIN 3 and CYSTATIN C proteins were induced by ADR in $p53^{+/+}$ cells (Figure 4, 8). *CYSTATIN C* mRNA was also induced by hydrogen peroxide in HCT116 $p53^{+/+}$ cells (Figure 9). I also confirmed the induction of *EPSIN 3* mRNA *and CYSTATIN C* mRNA by ADR treatment in MCF10A $p53^{+/+}$ normal breast epithelial cells but not in MCF10A $p53^{-/-}$ cells and (Figure 5, 10). I further verified that *CYSTATIN C* mRNAs were induced by ADR damage in HBC4 and HBL100 breast adenocarcinoma cell lines harboring wild-type *p53*, while *CYSTATIN C* induction was impaired by silencing of p53 (Figure 11).

To further evaluate the induction of EPSIN 3 and CYSTATIN C by p53, U373MG and H1299 cells were infected with Ad-p53 or Ad-LacZ. I found that mRNA and protein of both candidates were induced in cells infected with Ad-p53, indicating the regulation of EPSIN 3 and CYSTATIN C by p53 (Figure 6, 12). Then I measured the expression of both genes in $p53^{+/+}$ or $p53^{-/-}$ mice that were irradiated with 10 Gy of X-ray. At 24 h after irradiation, RNA purified from thymus were subjected to qPCR analysis. As a result, *Epsin 3* and *Cystatin C* mRNA were increased by X-ray irradiation in the thymus of $p53^{+/+}$ mice but not in the thymus of $p53^{-/-}$ mice (Figure 7, 13). These results clearly demonstrated the regulation of EPSIN 3 and CYSTATIN C by p53 *in vitro* and *in vivo*.

EPSIN 3 and CYSTATIN C is a direct target of p53

To investigate whether *EPSIN 3* and *CYSTATIN C* are direct targets of p53, I surveyed for p53-binding sequence (p53BS) [16] within their genetic loci and identified two potential binding sequences (p53BS1 and p53BS2) in the promoter region of *EPSIN 3* gene and one p53BS in first intron in *CYSTATIN C* gene (Figure 14). A 449-bases DNA fragment containing p53BS1 and p53BS2 of *EPSIN 3* (p53BS1+2) and 263-bases DNA

fragment containing p53BS of *CYSTATIN C* (p53BS) were amplified and subcloned upstream of the minimal promoter in pGL4.24 vector (pGL4.24/p53BS). The result of reporter assay revealed that U373MG cells transfected with pGL4.24/p53BS1+2 or pGL4.24/p53BS showed increased luciferase activity only in the presence of plasmid expressing wild-type p53 (Figure 15). However, base substitutions in the p53BS2 of *EPSIN 3* or p53BS of *CYSTATIN C* (pGL4.24/BSmut) completely diminished the enhancement of luciferase activity. These findings suggested that p53 transactivates *EPSIN 3* and *CYSTATIN C* through p53BS2 and p53BS, respectively. Since I generated *Epsin 3*-deficient mice, I also surveyed p53-binding sequence in mouse *Epsin 3* gene and found two potential binding sequences: mp53BS1 in promoter region, which was corresponding to human p53BS2, and mp53BS2 in the first intron. Of note, subsequent reporter assay revealed that luciferase activity was remarkably elevated in the cells transfected with pGL4.24/mp53BS2 rather than pGL4.24/mp53BS1 (Figure 16).

To verify whether p53 could directly bind to p53BSs, I performed ChIP assay using U373MG cells that were infected with either Ad-p53 or Ad-LacZ. After precipitation by an anti-p53 antibody, DNA fragments harboring p53BSs were quantified by qPCR. As a result, p53 specifically bound to p53BS2 (*EPSIN 3*) and p53BS (*CYSTATIN C*) in cells infected with Ad-p53 (Figure 17). Taken together, I concluded that *EPSIN 3* and *CYSTATIN C* are direct p53-targets.

Functional analysis of EPSIN 3

Epsins are accessory proteins implicated in clathrin-mediated endocytosis by binding ubiquitin moieties on the cytoplasmic part of membrane proteins. To date, three family members (EPSIN 1-3) have been identified in vertebrates. *EPSIN 1* and *EPSIN 2* are ubiquitously expressed in most type of tissues and were shown to be involved in the internalization of membrane proteins such as Notch ligands, eepithelial sodium channel,

epithelial growth factor receptor (EGFR), protease-activating receptor 1 and vascular endothelial growth factor 2 (VEGFR2) [29-33]. Targeted deletion of both *EPSIN 1* and *EPSIN 2* results in embryonic lethality due to defective vascular phenotype, suggesting that *EPSIN 1* and *EPSIN 2* play important and complementary roles in developmental stage [34]. In cancer tissues, there are growing evidences indicating up-regulation of *EPSIN 1* and *EPSIN 2* and their oncogenic implication [35]. EPSIN 1 promotes tumor angiogenesis regulating VEGF signaling pathway through internalization of VRGFR2 [33] and also endocytosis of Notch and Notch ligand. Besides internalization of membrane proteins, N-terminal ENTH domain of epsin activates GTPases, Rac1 and Arf6, through inhibition of RalBP1, a GTPase-activating protein (GAP), and subsequently results in actin remodeling and migration of cancer cells [33, 35]. As a novel function of epsins, a recent report showed that EPSIN 1 and EPSIN 2 interact with dishevelled2, a effecter protein of Wnt signaling, and prohibits its degradation, resulting in potentiating Wnt signaling and ensuing cancer progression [36].

In contrast to EPSIN 1 and EPSIN 2, the distribution of EPSIN 3 in mammalian body is highly limited. EPSIN 3 protein was shown to be expressed in the wounded keratinocytes and gastric parietal cells [37, 38]. Since EPSIN 3 share the major domains with the other family members, it has been expected that EPSIN 3 has also similar functions. However, the roles of this gene in both normal and cancer cells are largely unknown. Thus, I investigated the function of *EPSIN 3* as a p53-target.

EPSIN 3 is localized in inner surface of plasma membrane

To examine the subcellular localization of EPSIN 3, I performed immunocytochemistry using ADR-treated HCT116 $p53^{+/+}$ and $p53^{-/-}$ cells and HEK293T cells transfected with EPSIN 3 expressing plasmid. I found EPSIN 3 in the inner surface of plasma membrane of ADR-treated HCT116 $p53^{+/+}$ cells in which p53 were activated. On the other hand,

EPSIN 3 was rarely expressed in HCT116 *p53*$^{+/+}$ without ADR treatment or HCT116 *p53*$^{-/-}$ cells, consistent with the results of qPCR and western blot analysis (Figure 18). Ectopically expressed EPSIN 3 was also localized in inner surface of plasma membrane similar with EPSIN 1, suggesting that EPSIN 3 also interacts with membrane proteins (Figure 19).

Regulation of cancer cell growth and apoptosis by EPSIN 3

To explore the role of EPSIN 3 in the growth of cancer cells, I performed colony formation assay using three cancer cell lines: H1299, HCT116, and U373MG. As a results, colony formation was significantly impaired in HCT116 and U373MG cells which had been transfected with EPSIN 3 expressing plasmid compared with mock (Figure 20). Next, I designed four siRNAs (siEPN3-a-d) and found that both siEPN3-b and siEPN3-d effectively suppressed EPSIN 3 mRNA and protein (Figure 21). At the same time, I confirmed the specific protein bands of EPSIN 3. I subsequently analyzed cell viability by ATP measurement assay and found that EPSIN 3 knockdown inhibited the ADR-induced growth suppression to the same degree as cells treated with sip53 (Figure 22A). I further examined the impact of EPSIN 3 on ADR-induced apoptosis. Interestingly, knockdown of EPSIN 3 in ADR-treated HCT116 cells increased pro-caspase 3 and reduced cleaved caspase3, indicating the regulation of apoptosis by EPSIN 3 (Figure 22B).

Epsin 3-deficient mice show no phenotypic alterations

To investigate *in vivo* function of *Epsin 3*, I investigated *Epsin 3*- deficient mice. Frozen sperm purchased from knockout mouse project (KOMP) repository at UC Davis was recovered by using conventional *in vitro* fertilization and embryo transfer methods. Genotyping of new born mice were conducted by using specific primer set (Figure 23).

Firstly, I evaluated *Epsin 3* mRNA level of thymus tissue from 10 Gy of X-ray irradiated mice and confirmed not only knockout of the gene but induction by DNA damage in *Epsin 3*-wild-type mice (Figure 24A) . I next validated Epsin 3-knockout in protein level by western blot and immunohistochemistry using mouse stomach tissues (Figure 24B,C), in which protein expression of Epsin 3 is relatively higher than other tissues [38]. Unlike the previous study, where Epsin 3 was localized in gastric parietal cells [38], Epsin 3 was found in the whole of fundic glands in my immunohistochemistry study probably due to the specificity of the antibody. *Epsin 3*-deficient mice were born at the expected Mendelian frequency, had no obvious physiological defects and had no difference in biochemical analysis of blood samples compared to *Epsin 3*-wild-type mice.

In general, high dose X-ray irradiation causes depletion of bone marrow cells and subsequent death during 12-20 days after irradiation, while *p53*-deficient mice are resistant to the lethal myelosuppression, indicating a crucial role of p53 in genotoxic stress-mediated apoptosis of bone marrow cells [39]. Because I had demonstrated regulation of cell apoptosis through p53-EPSIN 3 pathway *in vitro*, I tested whether *Epsin 3* deficiency affects survival of X-ray irradiated mice. As a result, I found no significant difference between *Epsin 3*-wild-type and deficient mice in overall survival (Figure 25A). Next, I irradiated 6-weeks-old *Epsin 3*-wild-type or deficient mice with 4 Gy of X-ray for 4 times (once per week) to evaluate differences in tumor incidence. However, tumor free survival did not differ between the two groups (Figure 25B).

Because a previous report showed that EPSIN 3 was localized specifically to migrating keratinocytes in cutaneous wounds [37], I hypothesize that EPSIN 3 is involved in wound healing process. To test this hypothesis, I performed wound healing experiment using *Epsin 3*-deficient or wild-type mice. Contrary to my expectations, wound healing rates of *Epsin 3*-deficient mice were not different from those of *Epsin 3*-wild-type mice (Figure 26).

Down-regulation of EPSIN 3 in colorectal cancer

To address the involvement of EPSIN 3 in human carcinogenesis, I investigated the expression of *EPSIN 3* by using RNA sequence data of colorectal adenocarcinoma tissues released from the TCGA database [28]. Notably, expression of *EPSIN 3* was significantly decreased in colorectal adenocarcinoma tissues compared with the corresponding normal tissues (Figure 27). Taken together, the present findings would suggest the important role of *EPSIN 3* in colorectal carcinogenesis.

Functional analysis of CYSTATIN C

Cystatins are reversible, tight binding inhibitors against C1 cysteine proteases, which exert various physiological functions. Cystatin family members are categorized into three groups. Type 1 cystatins, also called stefins, are intracellular proteins which are present in most cells (cystatin A and B). Type 2 cystatins are secreted proteins found in most body fluids (CYSTATIN C, D, E/M, F, G, H, S, SA and SN). Type 3, also referred to as kininogens, are large multifunctional glycoproteins in body fluids, which work as acute phase proteins [40]. In the immune system, cystatins generally elicits immunosuppressive responses. Fetuin-A, a type 3 cystatin, down-regulates the pro-inflammatory cytokines and prevents excessive inflammation in wounded tissues [41, 42]. Type 2 cystatins inhibit autolysis of matrix metalloproteinases, which is an essential process for intact remodeling of the extracellular matrix [43]. CYSTATIN C, the most abundant type 2 cystatin, inhibits cathepsin L and S that are involved in antigen processing in antigen-presenting cells, resulting in suppression of MHC class II molecules-mediated immune responses [44].

Expression of cystatins in cancer tissues differs among the various cystatins, cancer types and clinical stages. For example, stefin A and B exhibited reduced

expression in breast cancer, malignant meningioma, and glioblastoma [45-49], while they were elevated in small cell or non-small cell lung cancer tissues [50, 51]. An inverse correlation between CYSTATIN C level and clinical stage of glioma and prostate cancer was demonstrated [52], while high serum CYSTATIN C level was shown to be associated with poor prognosis of colorectal cancer and melanoma [53, 54]. Thus the regulation of cystains and their roles in human carcinogenesis still remain unknown. I had identified CYSTATIN C as a p53-target and analyzed here the involvement of p53-CYSTATIN C pathway in cancer.

Regulation of cancer cell growth and apoptosis by CYSTATIN C

To explore the role of CYSTATIN C in the growth of cancer cells, I designed two siRNAs (siCystC-a and siCystC-b) and found that both siCystC-a and siCystC-b effectively suppressed CYSTATIN C mRNA and protein (Figure 28). I subsequently analyzed cell viability by ATP measurement assay and found that CYSTATIN C knockdown inhibited the ADR-induced growth suppression to the same degree as cells treated with sip53 (Figure 29A). Next, I examined the impact of CYSTATIN C on ADR-induced apoptosis. Interestingly, knockdown of CYSTATIN C in ADR-treated HCT116 cells increased pro-caspase 3 and reduced cleaved caspase 3, indicating the regulation of apoptosis by CYSTATIN C (Figure 29B).

Regulation of cathepsin L by p53-CYSTATIN C pathway

The lysosomal cysteine protease, cathepsin L, is an inhibitory target of CYSTATIN C [55]. Cathepsin L is highly expressed in various cancer cells and is involved in cancer development and progression [56, 57]. When HEK293T cells were transfected with plasmid expressing CYSTATIN C, cathepsin L activity was markedly decreased compared with mock-transfected cells (Figure 30A). Then I measured cathepsin L

activity in HCT116 *p53*$^{+/+}$ or *p53*$^{-/-}$ cells that were treated with ADR. As a result, cathepsin L activity was significantly reduced in HCT116 *p53*$^{+/+}$ cells after ADR treatment, while ADR treatment increased cathepsin L activity in *p53*$^{-/-}$ cells (Figure 30B). I further evaluated cathepsin L activity in HCT116 *p53*$^{+/+}$ that were treated with ADR at 24 h after transfection with siRNAs. As expected, p53 and CYSTATIN C knockdown resulted in increased activity of cathepsin L compared with control cells (Figure 30C). This result indicates that p53-CYSTATIN C pathway negatively regulates cathepsin L activity.

Regulation of CYSTATIN C by p53 in vivo

To explore the role of CYSTATIN C in human carcinogenesis, I investigated the expression of *CYSTATIN C* by using RNA sequence data of colorectal adenocarcinoma and breast adenocarcinoma tissues released from the TCGA database [28]. Notably, expression of *CYSTATIN C* was significantly decreased in both colorectal and breast adenocarcinoma tissues compared with the corresponding normal tissues (Figure 31). Moreover, *CYSTATIN C* expression in breast cancer tissues with *p53* mutation was significantly lower than those without *p53* mutation. Since *CYSTATIN C* expression was not reduced in breast cancer tissues with wild-type p53 compared to the corresponding normal tissues, p53 inactivation is likely to be the major cause of *CYSTATIN C* suppression in breast cancer tissues. I further assessed the impact of *CYSTATIN C* expression and *p53* mutation on clinical outcome by using the TCGA dataset. Concordant with the previous report [58, 59], breast cancer patients without *p53* mutation indicated better prognosis (Figure 32A). I also found that breast cancer patients with high *CYSTATIN C* expression exhibited significantly longer survival than those with low *CYSTATIN C* expression (Figure 32B). Moreover, multivariate analysis revealed that lower *CYSTATIN C* expression was an independent predictor of poor

prognosis in the patients with breast cancer (Table 2). Taken together, the results suggest that the p53-CYSTATIN C pathway plays an important role in the development and progression of human cancers.

Discussion

Here I identified EPSIN 3 and CYSTATIN C as novel p53 targets. Although several lines of evidence suggest that EPSIN 1 and 2 are implicated in carcinogenesis, I showed EPSIN 3 was induced by p53 and exerts tumor suppressive functions. Since epsin family members share structural similarities each other, it is difficult to explain functional diversities observed among them. However, my results of immunoblotting may provide some insights. There were two protein bands at approximately 75kDa (full-length size) and 40 kDa in the lane of whole cell lysate from HEK293T cells introduced with EPSIN 3, in contrast to that of EPSIN 1 in which only single band of full-length size was observed (Figure 19). This result indicates that EPSIN 3, not EPSIN 1, is cleaved into two parts. Further research is needed to elucidate the role of cleaved EPSIN 3.

In my analysis, I demonstrated that EPSIN 3 mediates apoptotic signaling in cancer cells. DNA damage provokes intrinsic apoptotic signaling cascade, in which a number of genes including known p53-targets form a complicated network [60]. Notably, knockdown of EPSIN 3 abrogated cleavage of caspase 3 as the same degree as p53-knockdown, suggesting that EPSIN 3 is involved in a common step in p53-caspase 3 axis. Among the known p53-targets involved in apoptosis, EPSIN 3 may play a pivotal role as one of the p53-induced apoptosis mediator.

Consistent with previous a report, my *Epsin 3*-deficient mice showed no pathological phenotypes. I speculated that it was because *Epsin 3* expression level was extremely low in most of organs. Therefore, I irradiated mice to induce *Epsin 3* expression in wild-type mice. However, there were no difference in survival and tumor development between *Epsin 3*-deficient and wild-type mice. This result could be partially explained by the fact that p53-binding sequence is not conserved between human and mice (Figure 16). Although human *EPSIN 3* is induced in many types of cell

lines, mouse *Epsin 3* was induced only in thymus. Therefore, regulatory mechanism as well as their physiological function would be different between human and mouse EPSIN 3.

CYSTATIN C is ubiquitously expressed in most organs and distributed in all body fluid compartments. Various physiological and pathological functions of CYSTATIN C have been reported such as apoptosis induction in neural cells, restriction of antigen presentation in antigen-presenting cells, and extracellular matrix remodeling [61]. In addition, several lines of evidence suggest the roles of CYSTATIN C in carcinogenesis. Down-regulation of CYSTATIN C in cancer tissues has repeatedly been reported [51, 62, 63], but the results are still controversial [64, 65]. So, I revealed that CYSTATIN C is a p53-downstream target which is involved in p53-induced apoptosis. The expression analysis using the TCGA database revealed that CYSTATIN C expression was negatively associated with *p53* mutation in cancer tissues. Since *p53* is frequently mutated in cancer tissues, down-regulation of CYSTATIN C in cancer tissues would mainly be caused by p53 inactivation.

I also showed that p53 negatively regulated cathepsin L activity in response to DNA damage. *p53* mutations in cancer tissues are associated with aggressive features and poor prognosis [66-72], but the molecular mechanism whereby p53 regulates cancer progression is not yet fully elucidated. Cathepsin L is one of the physiologically essential enzymes implicated in the degradation of extracellular matrix, modulation of immune response, and tissue development [73]. In cancer cells, cathepsin L was up-regulated, and its secreted form was shown to degradate extracellular matrix and promote cancer cell invasion [56, 74]. In addition, activated cathepsin L interferes with apoptosis of cancer cells [75]. Secreted CYSTATIN C was shown to be internalized into cancer cells and reduce cathepsin activity [76], and ectopically expressed CYSTATIN C reduced the invasiveness of melanoma cells [77]. Since cathepsin L activity is related

with tumor development and progression, the present findings suggested that negative regulation of cathepsin L by CYSTATIN C may play a crucial role in the tumor suppressive function of p53.

References

1. Baker, S.J., et al., *Chromosome 17 deletions and p53 gene mutations in colorectal carcinomas.* Science, 1989. **244**(4901): p. 217-21.
2. Eliyahu, D., et al., *Wild-type p53 can inhibit oncogene-mediated focus formation.* Proc Natl Acad Sci U S A, 1989. **86**(22): p. 8763-7.
3. Finlay, C.A., P.W. Hinds, and A.J. Levine, *The p53 proto-oncogene can act as a suppressor of transformation.* Cell, 1989. **57**(7): p. 1083-93.
4. Montes de Oca Luna, R., D.S. Wagner, and G. Lozano, *Rescue of early embryonic lethality in mdm2-deficient mice by deletion of p53.* Nature, 1995. **378**(6553): p. 203-6.
5. Ringshausen, I., et al., *Mdm2 is critically and continuously required to suppress lethal p53 activity in vivo.* Cancer Cell, 2006. **10**(6): p. 501-14.
6. Appella, E. and C.W. Anderson, *Post-translational modifications and activation of p53 by genotoxic stresses.* Eur J Biochem, 2001. **268**(10): p. 2764-72.
7. Al Rashid, S.T., et al., *Protein-protein interactions occur between p53 phosphoforms and ATM and 53BP1 at sites of exogenous DNA damage.* Radiat Res, 2011. **175**(5): p. 588-98.
8. Dumaz, N., D.M. Milne, and D.W. Meek, *Protein kinase CK1 is a p53-threonine 18 kinase which requires prior phosphorylation of serine 15.* FEBS Lett, 1999. **463**(3): p. 312-6.
9. Dumaz, N., et al., *Critical roles for the serine 20, but not the serine 15, phosphorylation site and for the polyproline domain in regulating p53 turnover.* Biochem J, 2001. **359**(Pt 2): p. 459-64.
10. Caron de Fromentel, C. and T. Soussi, *TP53 tumor suppressor gene: a model for investigating human mutagenesis.* Genes Chromosomes Cancer, 1992. **4**(1): p. 1-15.
11. Levine, A.J. and M. Oren, *The first 30 years of p53: growing ever more complex.* Nat Rev Cancer, 2009. **9**(10): p. 749-58.

12. Tanikawa, C., et al., *Regulation of protein Citrullination through p53/PADI4 network in DNA damage response.* Cancer Res, 2009. **69**(22): p. 8761-9.

13. Soussi, T. and K.G. Wiman, *Shaping genetic alterations in human cancer: the p53 mutation paradigm.* Cancer Cell, 2007. **12**(4): p. 303-12.

14. Kilpivaara, O. and L.A. Aaltonen, *Diagnostic cancer genome sequencing and the contribution of germline variants.* Science, 2013. **339**(6127): p. 1559-62.

15. Petitjean, A., et al., *Impact of mutant p53 functional properties on TP53 mutation patterns and tumor phenotype: lessons from recent developments in the IARC TP53 database.* Hum Mutat, 2007. **28**(6): p. 622-9.

16. el-Deiry, W.S., et al., *Definition of a consensus binding site for p53.* Nat Genet, 1992. **1**(1): p. 45-9.

17. Kato, S., et al., *Understanding the function-structure and function-mutation relationships of p53 tumor suppressor protein by high-resolution missense mutation analysis.* Proc Natl Acad Sci U S A, 2003. **100**(14): p. 8424-9.

18. Tokino, T., et al., *p53 tagged sites from human genomic DNA.* Hum Mol Genet, 1994. **3**(9): p. 1537-42.

19. Oda, K., et al., *p53AIP1, a potential mediator of p53-dependent apoptosis, and its regulation by Ser-46-phosphorylated p53.* Cell, 2000. **102**(6): p. 849-62.

20. Liang, P. and A.B. Pardee, *Differential display of eukaryotic messenger RNA by means of the polymerase chain reaction.* Science, 1992. **257**(5072): p. 967-71.

21. Tanaka, H., et al., *A ribonucleotide reductase gene involved in a p53-dependent cell-cycle checkpoint for DNA damage.* Nature, 2000. **404**(6773): p. 42-9.

22. Ono, K., et al., *Identification by cDNA microarray of genes involved in ovarian carcinogenesis.* Cancer Res, 2000. **60**(18): p. 5007-11.

23. Tanikawa, C., et al., *p53RDL1 regulates p53-dependent apoptosis.* Nat Cell Biol, 2003. **5**(3): p. 216-23.

24. Tanikawa, C., et al., *XEDAR as a putative colorectal tumor suppressor that*

mediates p53-regulated anoikis pathway. Oncogene, 2009. **28**(34): p. 3081-92.

25. Funauchi, Y., et al., *Regulation of iron homeostasis by the p53-ISCU pathway.* Sci Rep, 2015. **5**: p. 16497.

26. Ueda, K., et al., *Antibody-coupled monolithic silica microtips for highthroughput molecular profiling of circulating exosomes.* Sci Rep, 2014. **4**: p. 6232.

27. Tsukada, T., et al., *Enhanced proliferative potential in culture of cells from p53-deficient mice.* Oncogene, 1993. **8**(12): p. 3313-22.

28. *The Cancer Genome Atlus.* [cited 2015 15 May]; Available from: https://tcga-data.nci.nih.gov.

29. Kazazic, M., et al., *Epsin 1 is involved in recruitment of ubiquitinated EGF receptors into clathrin-coated pits.* Traffic, 2009. **10**(2): p. 235-45.

30. Chen, B., et al., *Adaptor protein complex-2 (AP-2) and epsin-1 mediate protease-activated receptor-1 internalization via phosphorylation- and ubiquitination-dependent sorting signals.* J Biol Chem, 2011. **286**(47): p. 40760-70.

31. Wang, W. and G. Struhl, *Drosophila Epsin mediates a select endocytic pathway that DSL ligands must enter to activate Notch.* Development, 2004. **131**(21): p. 5367-80.

32. Wang, H., et al., *Clathrin-mediated endocytosis of the epithelial sodium channel. Role of epsin.* J Biol Chem, 2006. **281**(20): p. 14129-35.

33. Pasula, S., et al., *Endothelial epsin deficiency decreases tumor growth by enhancing VEGF signaling.* J Clin Invest, 2012. **122**(12): p. 4424-38.

34. Chen, H., et al., *Embryonic arrest at midgestation and disruption of Notch signaling produced by the absence of both epsin 1 and epsin 2 in mice.* Proc Natl Acad Sci U S A, 2009. **106**(33): p. 13838-43.

35. Tessneer, K.L., et al., *Endocytic adaptor protein epsin is elevated in prostate cancer and required for cancer progression.* ISRN Oncol, 2013. **2013**: p. 420597.

36. Chang, B., et al., *Epsin is required for Dishevelled stability and Wnt signalling activation in colon cancer development.* Nat Commun, 2015. **6**: p. 6380.

37. Spradling, K.D., et al., *Epsin 3 is a novel extracellular matrix-induced transcript specific to wounded epithelia.* J Biol Chem, 2001. **276**(31): p. 29257-67.

38. Ko, G., et al., *Selective high-level expression of epsin 3 in gastric parietal cells, where it is localized at endocytic sites of apical canaliculi.* Proc Natl Acad Sci U S A, 2010. **107**(50): p. 21511-6.

39. Komarova, E.A., et al., *Dual effect of p53 on radiation sensitivity in vivo: p53 promotes hematopoietic injury, but protects from gastro-intestinal syndrome in mice.* Oncogene, 2004. **23**(19): p. 3265-71.

40. Ochieng, J. and G. Chaudhuri, *Cystatin superfamily.* J Health Care Poor Underserved, 2010. **21**(1 Suppl): p. 51-70.

41. Wang, H., et al., *Fetuin protects the fetus from TNF.* Lancet, 1997. **350**(9081): p. 861-2.

42. Zhang, M., et al., *Spermine inhibits proinflammatory cytokine synthesis in human mononuclear cells: a counterregulatory mechanism that restrains the immune response.* J Exp Med, 1997. **185**(10): p. 1759-68.

43. Ray, S., P. Lukyanov, and J. Ochieng, *Members of the cystatin superfamily interact with MMP-9 and protect it from autolytic degradation without affecting its gelatinolytic activities.* Biochim Biophys Acta, 2003. **1652**(2): p. 91-102.

44. Pierre, P. and I. Mellman, *Developmental regulation of invariant chain proteolysis controls MHC class II trafficking in mouse dendritic cells.* Cell, 1998. **93**(7): p. 1135-45.

45. Hawley-Nelson, P., et al., *Molecular cloning of mouse epidermal cystatin A and detection of regulated expression in differentiation and tumorigenesis.* Mol Carcinog, 1988. **1**(3): p. 202-11.

46. Zajc, I., et al., *Expression of cysteine peptidase cathepsin L and its inhibitors stefins A and B in relation to tumorigenicity of breast cancer cell lines.* Cancer Lett, 2002. **187**(1-2): p. 185-90.

47. Strojnik, T., et al., *Cathepsins B and L are markers for clinically invasive types of meningiomas.* Neurosurgery, 2001. **48**(3): p. 598-605.

48. Strojnik, T., T.T. Lah, and B. Zidanik, *Immunohistochemical staining of cathepsins B, L and stefin A in human hypophysis and pituitary adenomas.* Anticancer Res, 2005. **25**(1B): p. 587-94.

49. Levicar, N., et al., *Lysosomal enzymes, cathepsins in brain tumour invasion.* J Neurooncol, 2002. **58**(1): p. 21-32.

50. Heidtmann, H.H., et al., *Cathepsin B and cysteine proteinase inhibitors in human lung cancer cell lines.* Clin Exp Metastasis, 1997. **15**(4): p. 368-81.

51. Werle, B., et al., *Cystatins in non-small cell lung cancer: tissue levels, localization and relation to prognosis.* Oncol Rep, 2006. **16**(4): p. 647-55.

52. Jiborn, T., et al., *Aberrant expression of cystatin C in prostate cancer is associated with neuroendocrine differentiation.* BJU Int, 2006. **98**(1): p. 189-96.

53. Kos, J., et al., *Cysteine proteinase inhibitors stefin A, stefin B, and cystatin C in sera from patients with colorectal cancer: relation to prognosis.* Clin Cancer Res, 2000. **6**(2): p. 505-11.

54. Kos, J., et al., *Cathepsins B, H, and L and their inhibitors stefin A and cystatin C in sera of melanoma patients.* Clin Cancer Res, 1997. **3**(10): p. 1815-22.

55. Barrett, A.J., M.E. Davies, and A. Grubb, *The place of human gamma-trace (cystatin C) amongst the cysteine proteinase inhibitors.* Biochem Biophys Res Commun, 1984. **120**(2): p. 631-6.

56. Lankelma, J.M., et al., *Cathepsin L, target in cancer treatment?* Life Sci, 2010. **86**(7-8): p. 225-33.

57. Turk, V., et al., *Human cysteine proteinases and their protein inhibitors stefins, cystatins and kininogens.* Biomed Biochim Acta, 1986. **45**(11-12): p. 1375-84.

58. Olivier, M., et al., *The clinical value of somatic TP53 gene mutations in 1,794 patients with breast cancer.* Clin Cancer Res, 2006. **12**(4): p. 1157-67.

59. Kovach, J.S., et al., *Mutation detection by highly sensitive methods indicates that p53 gene mutations in breast cancer can have important prognostic value.* Proc Natl Acad Sci U S A, 1996. **93**(3): p. 1093-6.

60. Haupt, S., et al., *Apoptosis - the p53 network.* J Cell Sci, 2003. **116**(Pt 20): p. 4077-85.

61. Xu, Y., et al., *Cystatin C is a disease-associated protein subject to multiple regulation.* Immunol Cell Biol, 2015. **93**(5): p. 442-451.

62. Wegiel, B., et al., *Cystatin C is downregulated in prostate cancer and modulates invasion of prostate cancer cells via MAPK/Erk and androgen receptor pathways.* PLoS One, 2009. **4**(11): p. e7953.

63. Sokol, J.P. and W.P. Schiemann, *Cystatin C antagonizes transforming growth factor beta signaling in normal and cancer cells.* Mol Cancer Res, 2004. **2**(3): p. 183-95.

64. Zeng, Q., et al., *Expression of Cystatin C in human stomach neoplasms.* Mol Med Rep, 2010. **3**(4): p. 607-11.

65. Zeng, Q., et al., *Expression of cystatin C in human esophageal cancer.* Tumori, 2011. **97**(2): p. 203-10.

66. Dicker, F., et al., *The detection of TP53 mutations in chronic lymphocytic leukemia independently predicts rapid disease progression and is highly correlated with a complex aberrant karyotype.* Leukemia, 2009. **23**(1): p. 117-24.

67. Young, K.H., et al., *Structural profiles of TP53 gene mutations predict clinical outcome in diffuse large B-cell lymphoma: an international collaborative study.* Blood, 2008. **112**(8): p. 3088-98.

68. Pricolo, V.E., et al., *Mutated p53 gene is an independent adverse predictor of survival in colon carcinoma.* Arch Surg, 1997. **132**(4): p. 371-4; discussion 374-5.

69. Marchetti, A., et al., *p53 alterations in non-small cell lung cancers correlate with metastatic involvement of hilar and mediastinal lymph nodes.* Cancer Res, 1993. **53**(12): p. 2846-51.

70. Bardeesy, N., et al., *Anaplastic Wilms' tumour, a subtype displaying poor prognosis, harbours p53 gene mutations.* Nat Genet, 1994. **7**(1): p. 91-7.

71. Aas, T., et al., *Specific P53 mutations are associated with de novo resistance to doxorubicin in breast cancer patients.* Nat Med, 1996. **2**(7): p. 811-4.

72. Erber, R., et al., *TP53 DNA contact mutations are selectively associated with allelic loss and have a strong clinical impact in head and neck cancer.* Oncogene, 1998. **16**(13): p. 1671-9.

73. Turk, V., et al., *Cysteine cathepsins: from structure, function and regulation to new frontiers.* Biochim Biophys Acta, 2012. **1824**(1): p. 68-88.

74. Fonovic, M. and B. Turk, *Cysteine cathepsins and extracellular matrix degradation.* Biochim Biophys Acta, 2014. **1840**(8): p. 2560-70.

75. Levicar, N., et al., *Selective suppression of cathepsin L by antisense cDNA impairs human brain tumor cell invasion in vitro and promotes apoptosis.* Cancer Gene Ther, 2003. **10**(2): p. 141-51.

76. Wallin, H., M. Abrahamson, and U. Ekstrom, *Cystatin C properties crucial for uptake and inhibition of intracellular target enzymes.* J Biol Chem, 2013. **288**(23): p. 17019-29.

77. Cox, J.L., et al., *Inhibition of B16 melanoma metastasis by overexpression of the cysteine proteinase inhibitor cystatin C.* Melanoma Res, 1999. **9**(4): p. 369-74.

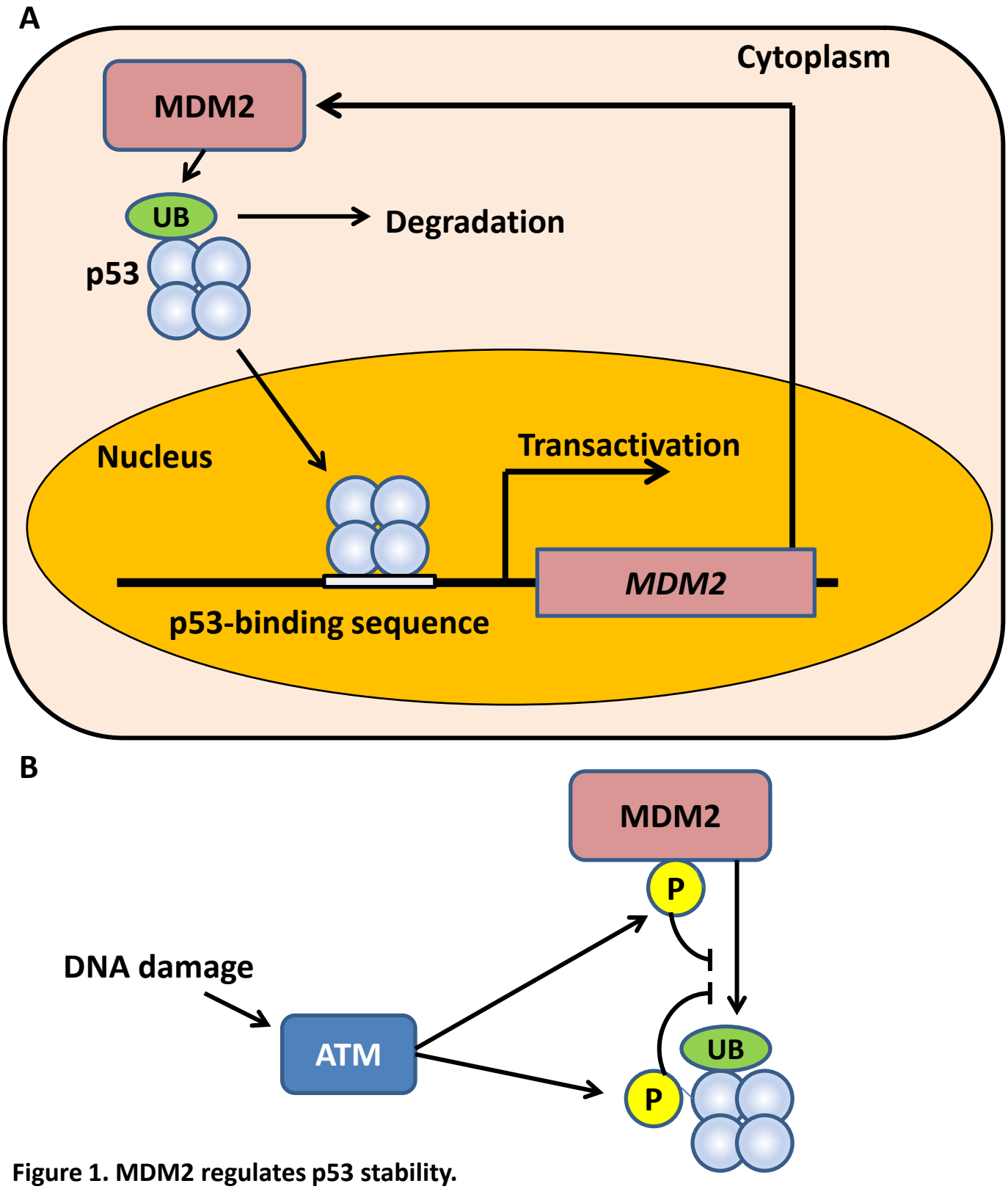

Figure 1. MDM2 regulates p53 stability.
(A) MDM2-p53 constitutes a negative feedback loop. Green ellipse indicates ubiquitilytion of p53 protein, leading to its degradation. (B) Cellular stresses induces ATM , a protein kinase, which phosphorylates MDM2 and p53 (yellow circles), resulting in preventing interaction of MDM2 with p53.

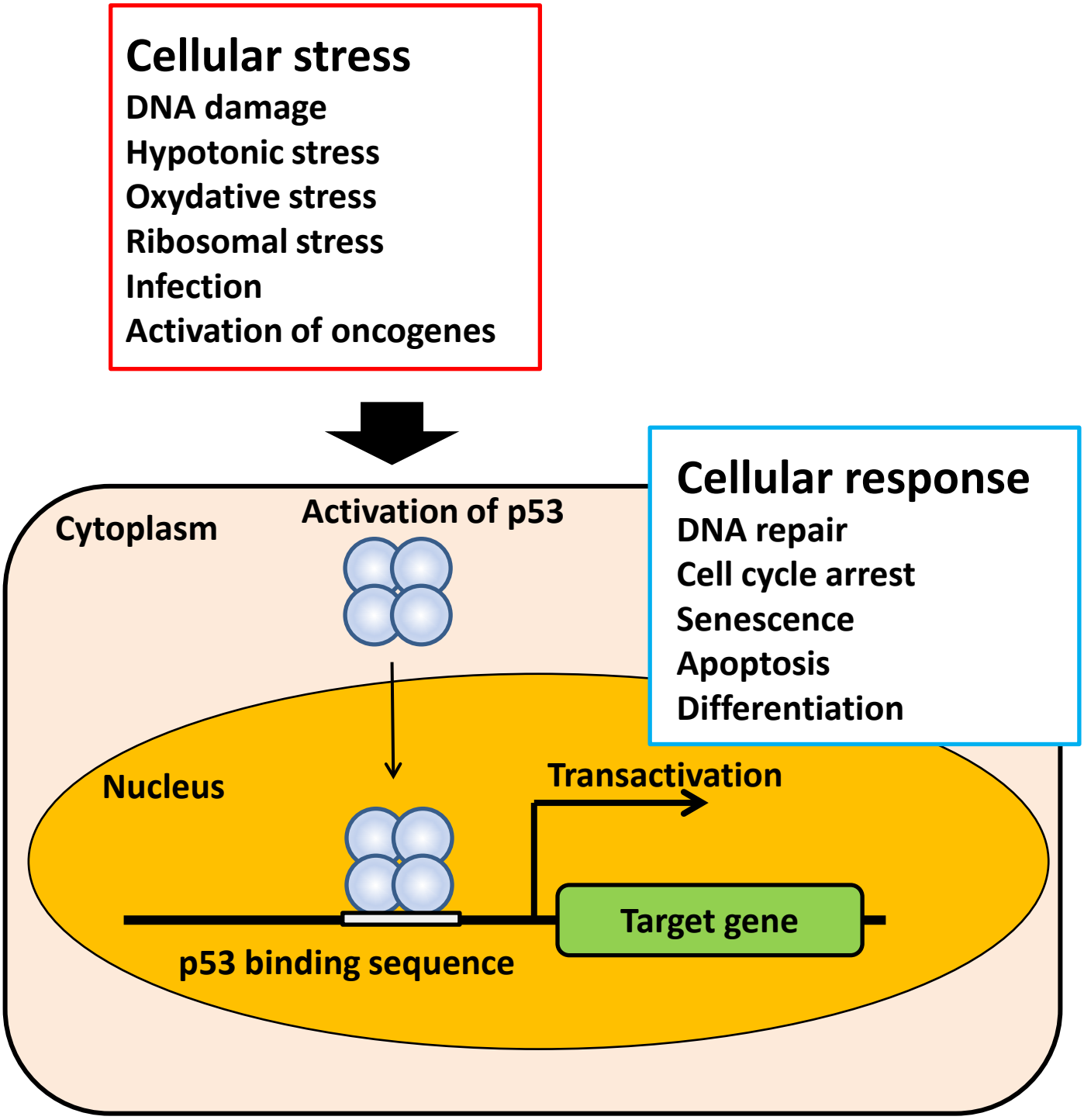

Figure 2. Schematic of p53-mediated responses after cellular stresses.
Various cellular stresses shown in the red box induce p53 activation. Activated p53 binds to the region of target genes thoμgh specific p53-binding sequence, and thereby transcription of the gene exerts tumor suppressive response shown in the blue box.

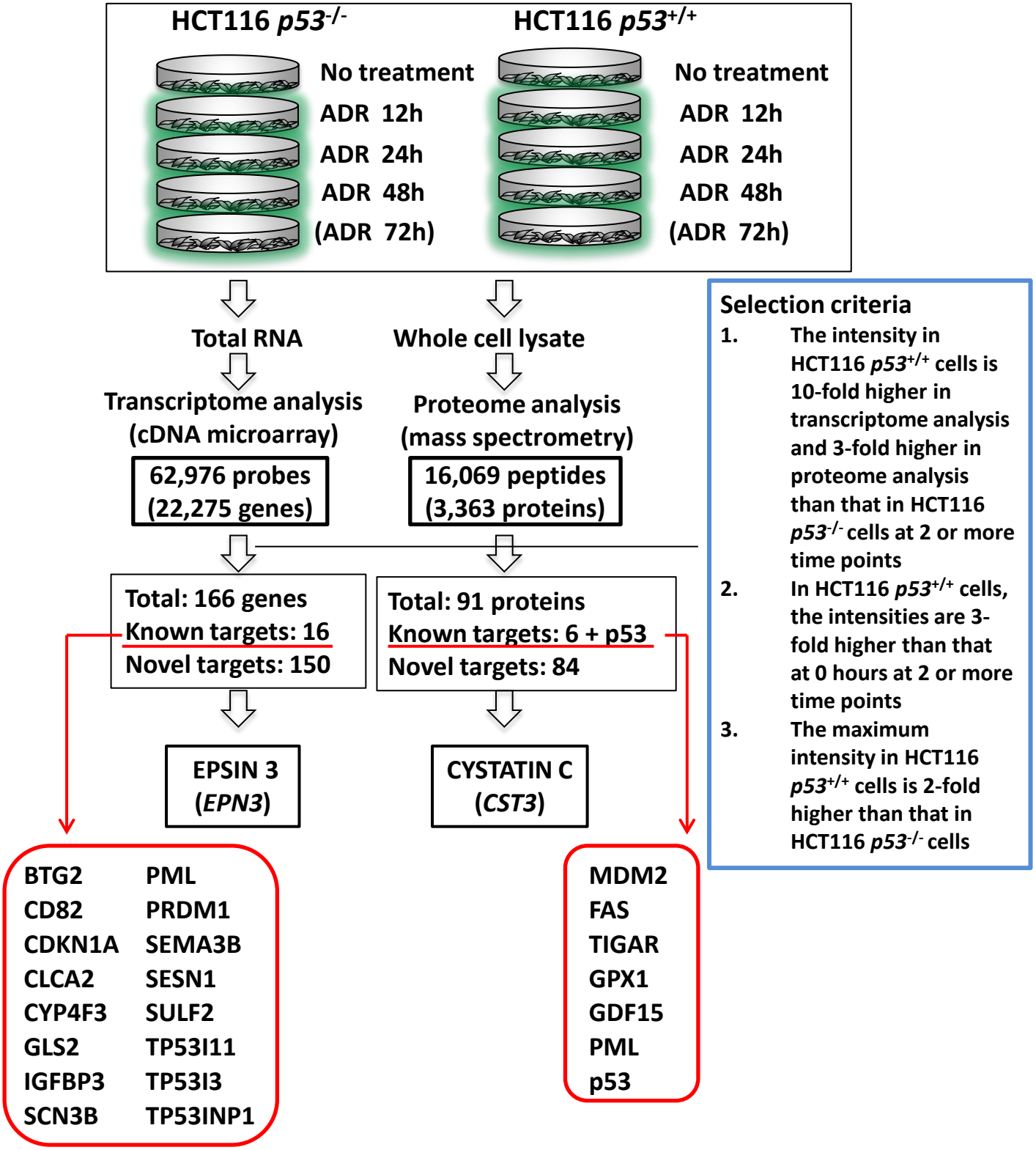

Figure 3. Schematic diagram of screening methodology of p53-inducible targets.
HCT116 *p53*$^{-/-}$ or *p53*$^{+/+}$ cells harvested at the indicated times after 2 μg/ml ADR treatment for 2 h were subjected to transcriptome and proteome analysis. The selection criteria in the blue box was used to extract p53-inducible targets from the Raw data. Gene names of known p53-targets screened by each method were shown in the red boxes.

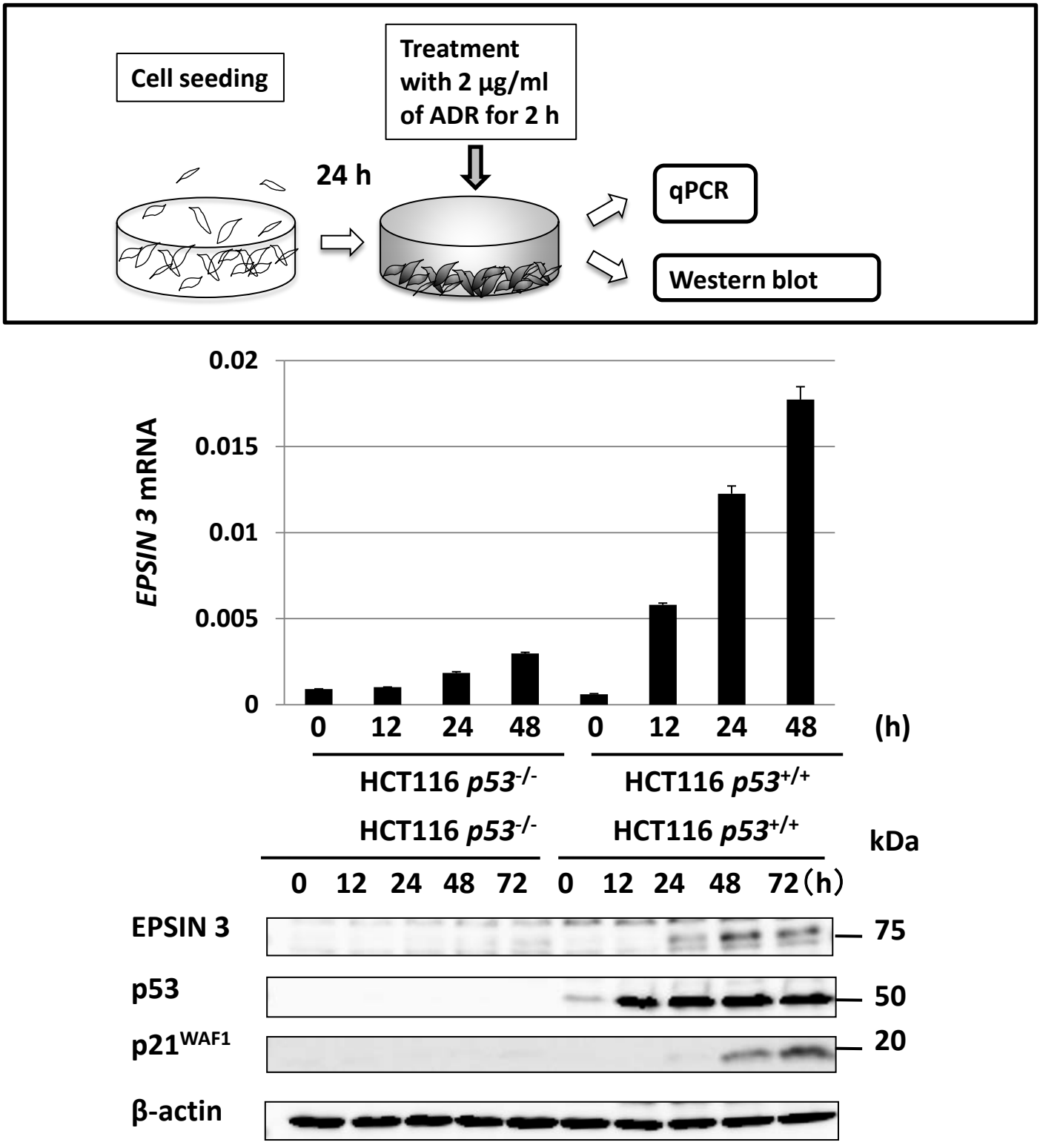

Figure 4. Induction of CYSTATIN C by DNA damage.
qPCR analysis of EPSIN 3 in HCT116 *p53*$^{-/-}$ or *p53*$^{+/+}$ cells harvested at the indicated times after 2 μg/ml ADR treatment for 2 h (upper). *β-actin* was used for the normalization of expression levels. Error bars represent S.D. (n = 3). HCT116 *p53*$^{-/-}$ or HCT116 *p53*$^{+/+}$ cells were treated with 2 μg/ml ADR for 2 h. At the indicated times after the treatment, whole cell extracts were subjected to immunoblotting using anti-CYSTATIN C, anti-p53, anti-p21, or anti-actin antibody (lower)

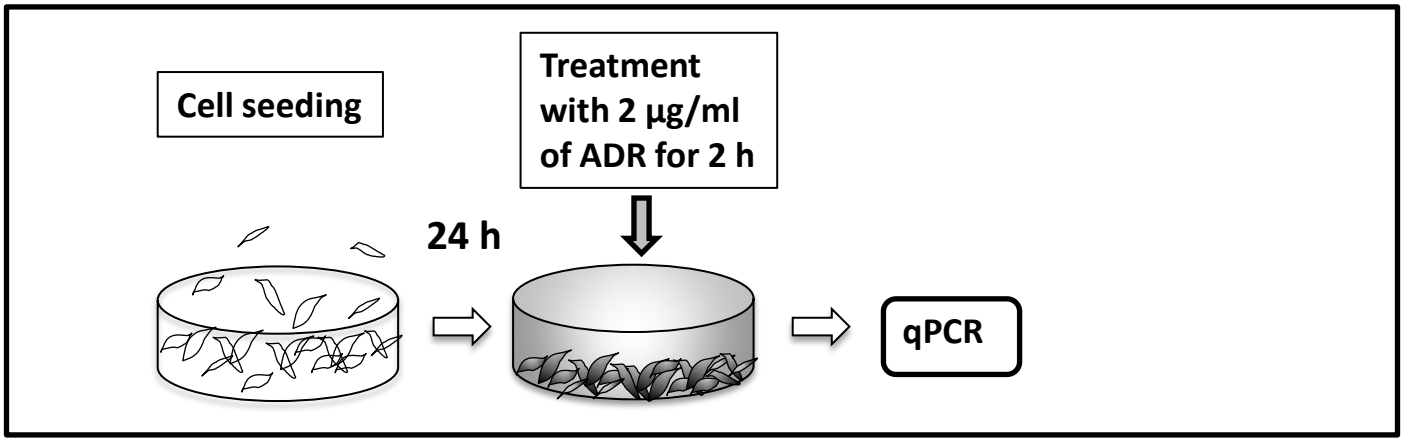

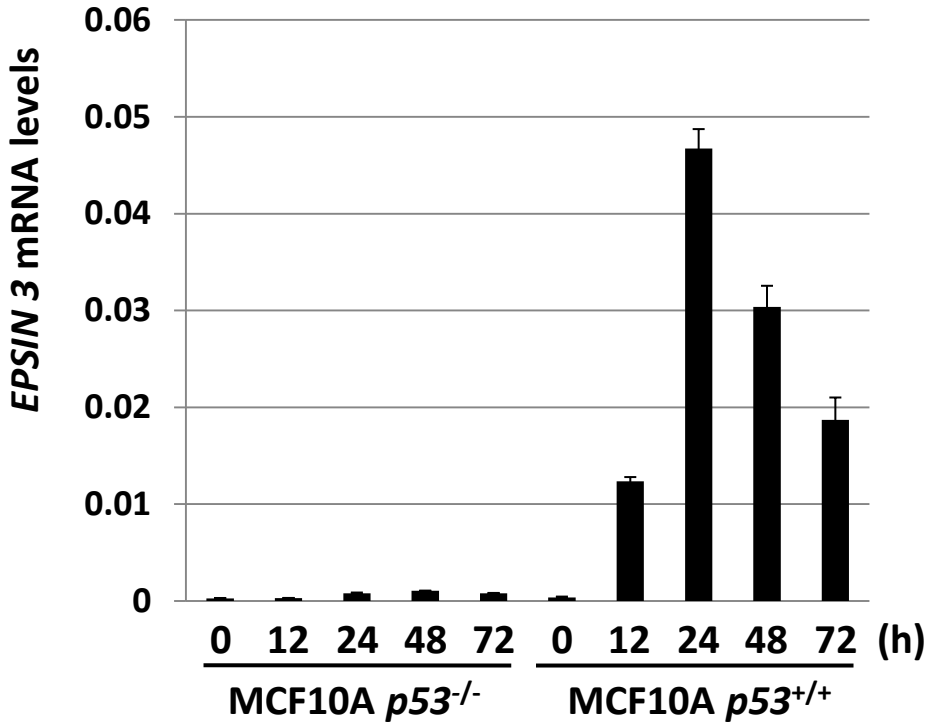

Figure 5. Induction of *EPSIN 3* by DNA damage in mammalian cells
qPCR analysis of *EPSIN 3* in MCF10A *p53*$^{-/-}$ or *p53*$^{+/+}$ cells harvested at the indicated times after 2 µg/ml ADR treatment for 2 h. *β-actin* was used for the normalization of expression levels. Error bars represent S.D. (n = 2).

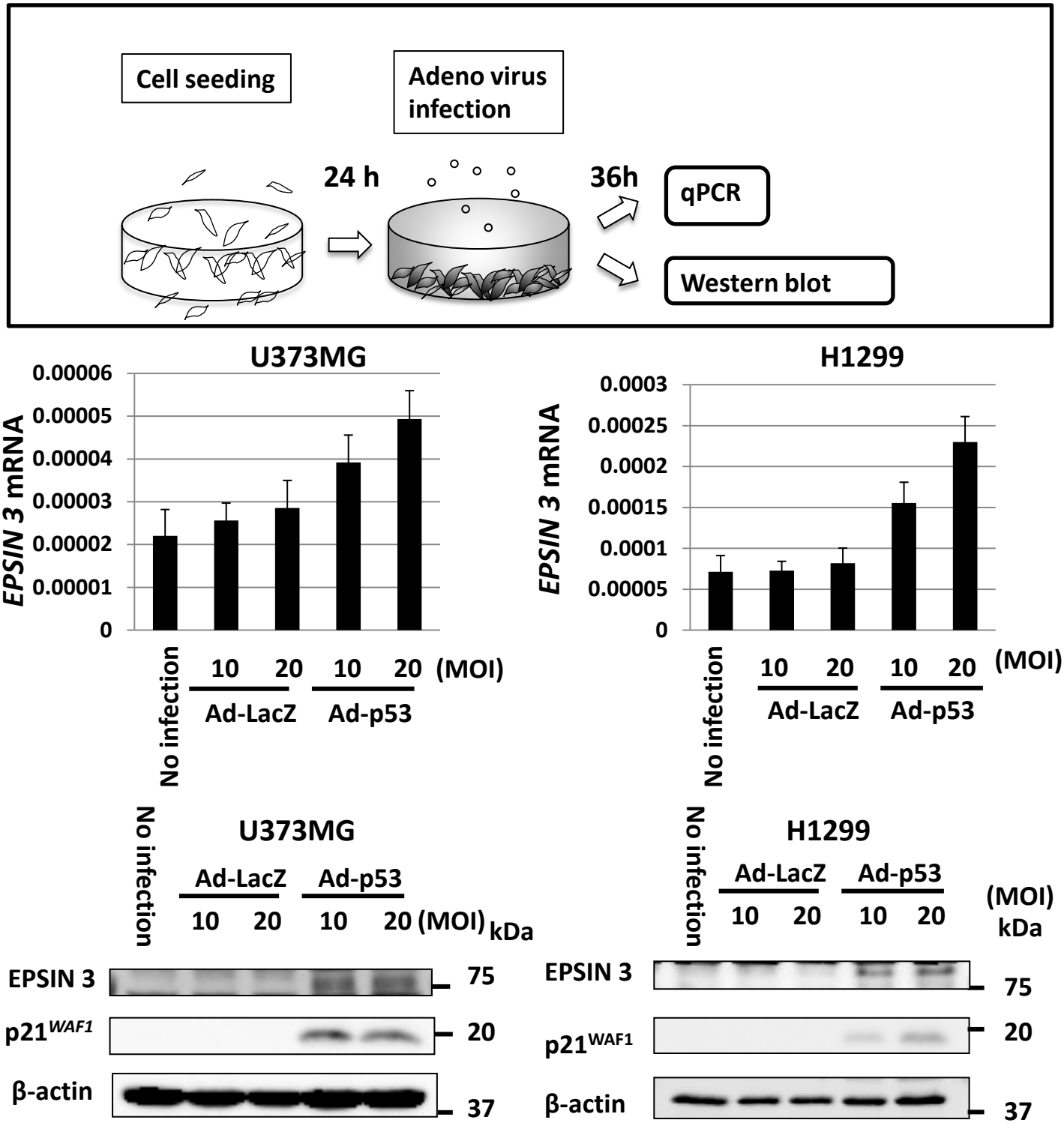

Figure 6. Induction of EPSIN 3 by p53.

(Upper) qPCR analysis of *EPSIN 3* in U373MG (*p53* mutant) and H1299 (*p53* null) cells infected with adenovirus expressing p53 (Ad-p53) or LacZ (Ad-LacZ) at multiplicity of infection (MOI) of 10 or 20. *β-actin* was used for the normalization of expression levels. Error bars represent S.D. (n = 3). (lower) U373MG cells and H1299 were infected with Ad-p53 or Ad-LacZ at MOI of 10 or 20. At 36 h after treatment, whole cell extracts were subjected to Western blot with anti-EPSIN 3, anti-p21, or anti-actin antibody

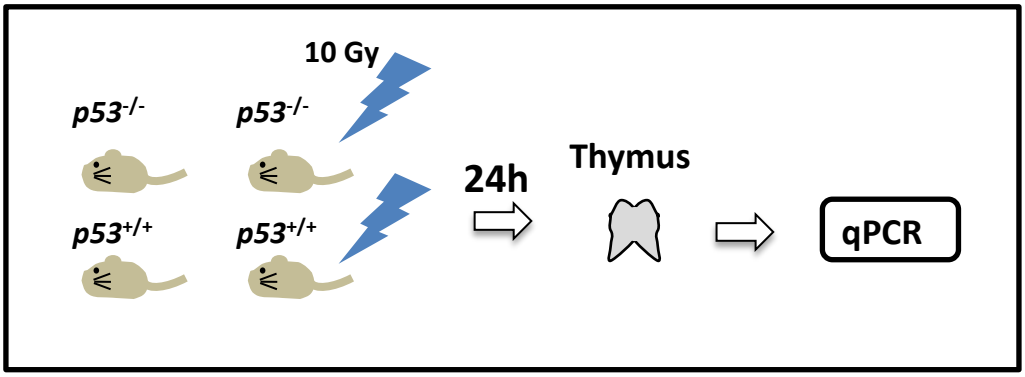

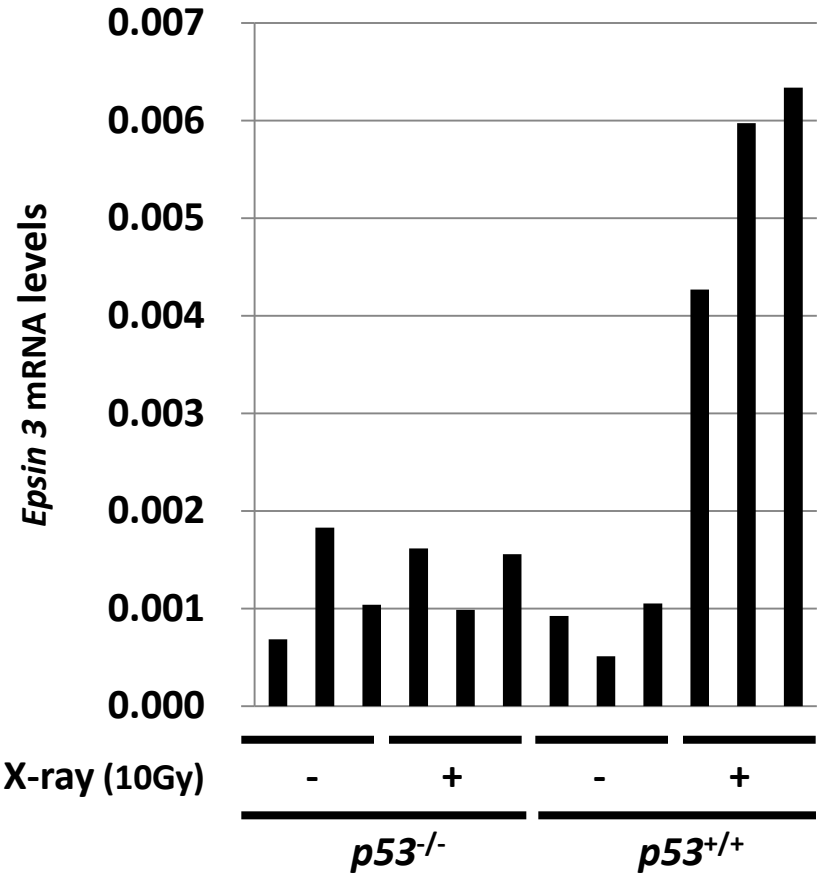

Figure 7. Induction of *Epsin 3* by DNA damage in mouse tissues
qPCR analysis of *Epsin 3* expression in the thymus of X-ray-irradiated $p53^{-/-}$ or $p53^{+/+}$ mice (10 Gy) (n=3 per group). *β-actin* was used for the normalization of expression levels. Mice were sacrificed 24 h after irradiation with 10 Gy of X-ray.

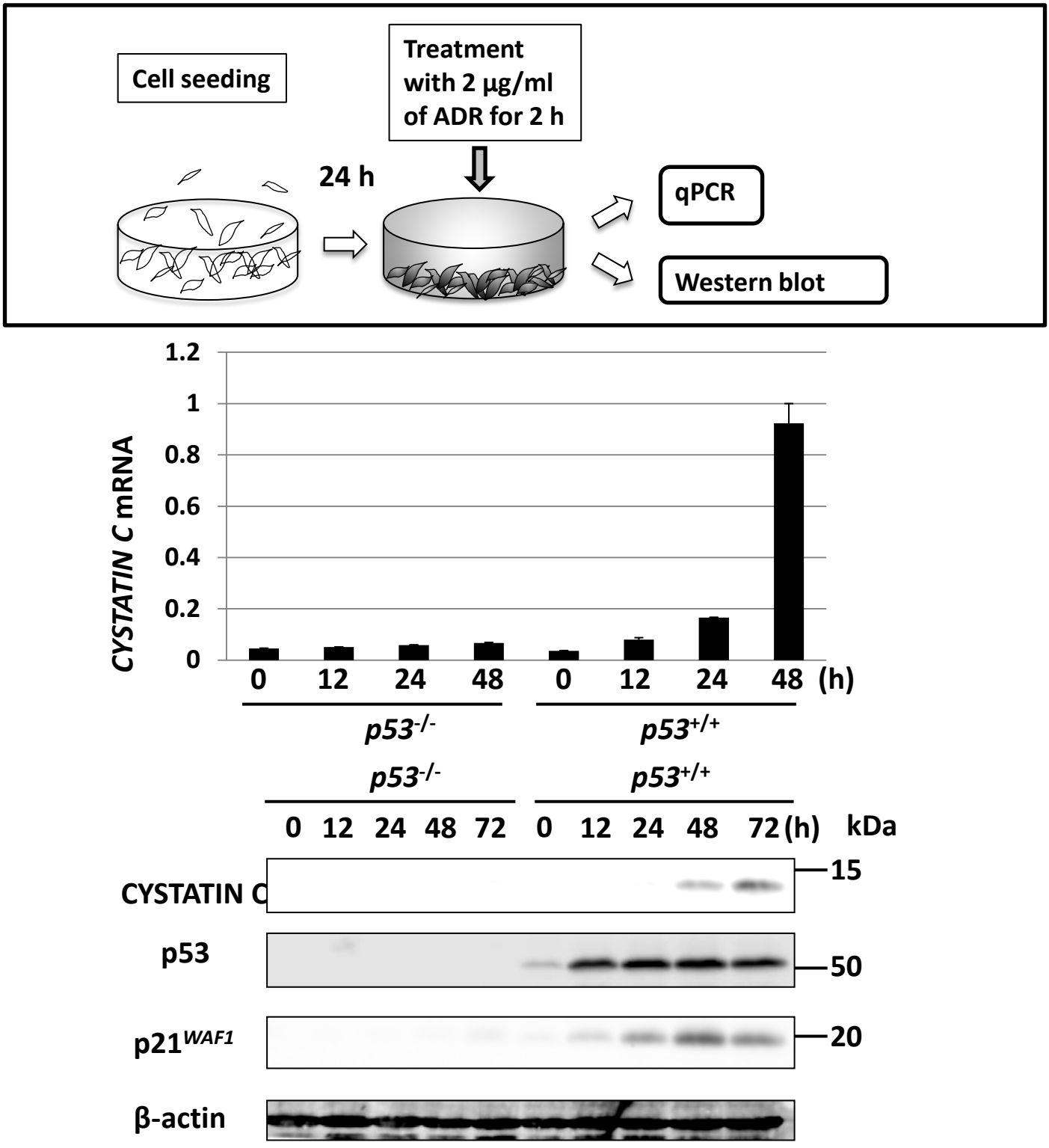

Figure 8. Induction of CYSTATIN C by DNA damage.

qPCR analysis of CYSTATIN C in HCT116 *p53*$^{-/-}$ or *p53*$^{+/+}$ cells harvested at the indicated times after 2 μg/ml ADR treatment for 2 h (upper). *β-actin* was used for the normalization of expression levels. Error bars represent S.D. (n = 3). HCT116 *p53*$^{-/-}$ or HCT116 *p53*$^{+/+}$ cells were treated with 2 μg/ml ADR for 2 h. At the indicated times after the treatment, whole cell extracts were subjected to Western blot using anti-CYSTATIN C, anti-p53, anti-p21, or anti-actin antibody (lower)

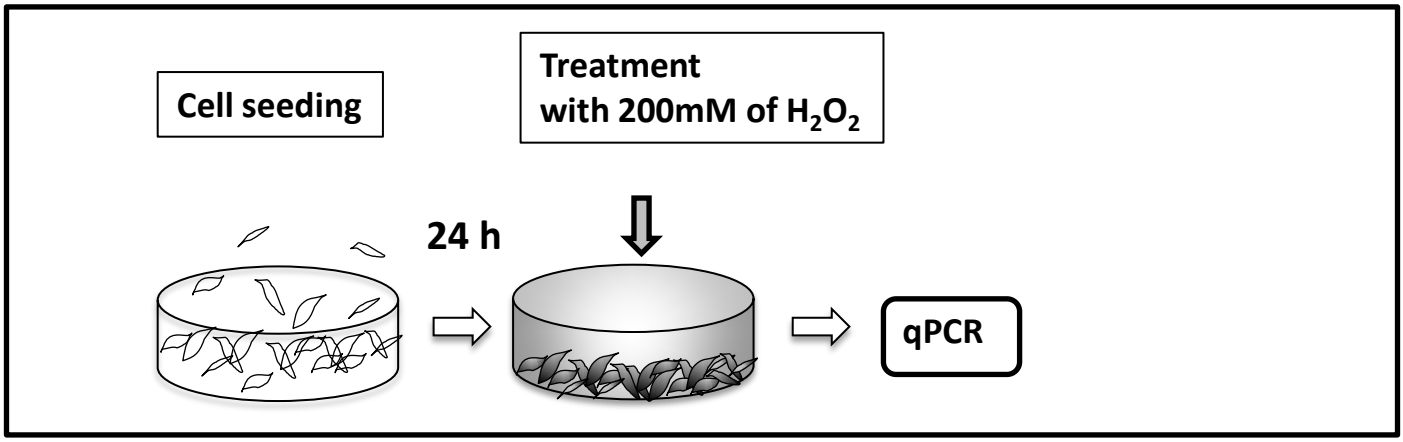

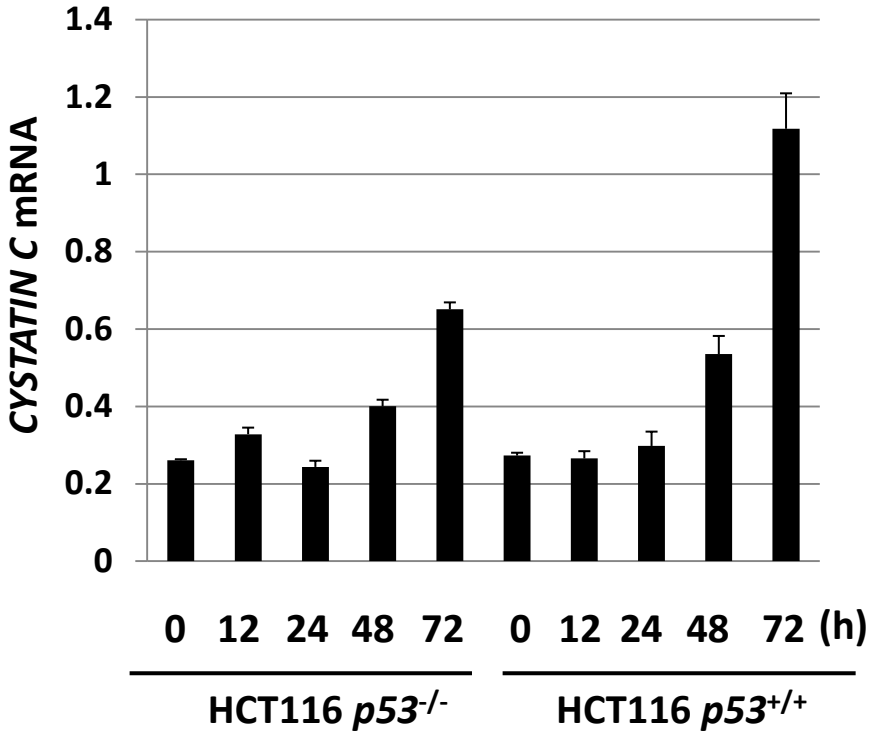

Figure 9. Induction of CYSTATIN C by oxydative stress.
HCT116 *p53*$^{-/-}$ or HCT116 *p53*$^{+/+}$ cells were treated with 200mM H2O2. At the indicated times after treatment, qPCR analysis was performed. *β-actin* was used for the normalization of expression levels. Error bars represent S.D. (n = 3)

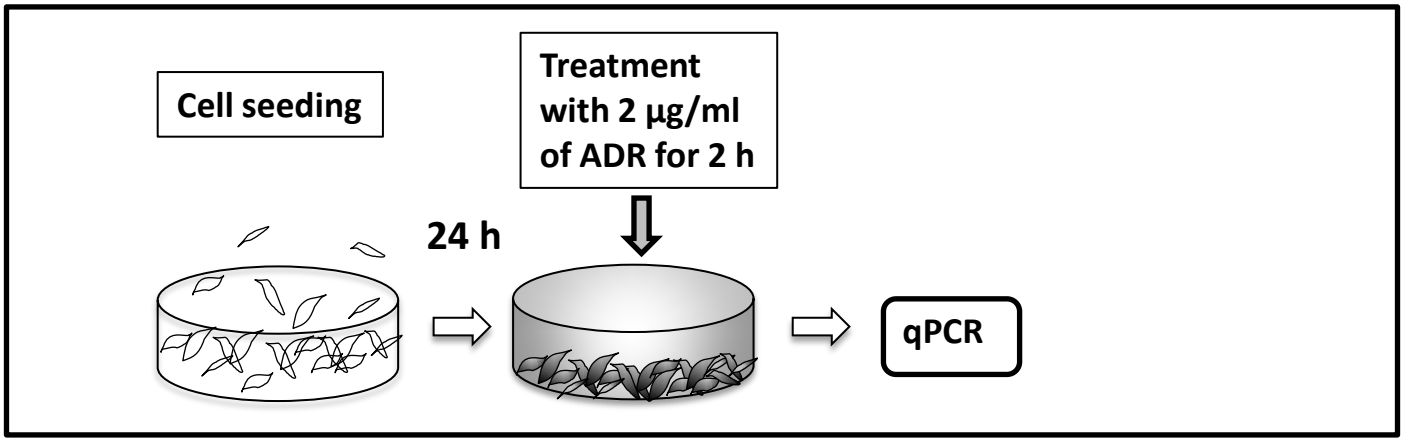

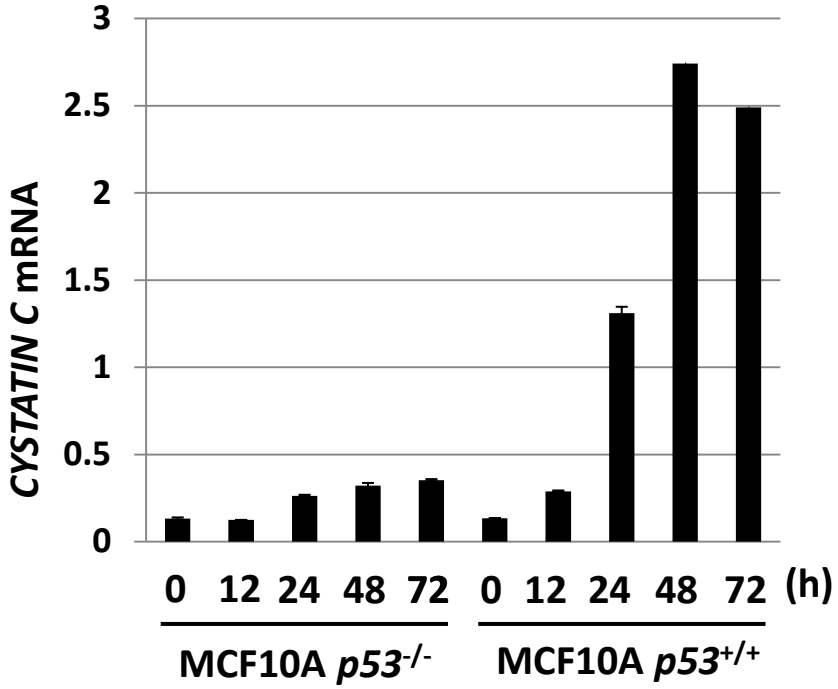

Figure 10. Induction of CYSTATIN C by DNA damage in normal mammalian cells and breast cancer cells

qPCR analysis of *CYSTATIN C* in MCF10A $p53^{-/-}$ or $p53^{+/+}$ cells harvested at the indicated times after 2 μg/ml of ADR treatment for 2 h. *β-actin* was used for the normalization of expression levels. Error bars represent S.D. (n = 3).

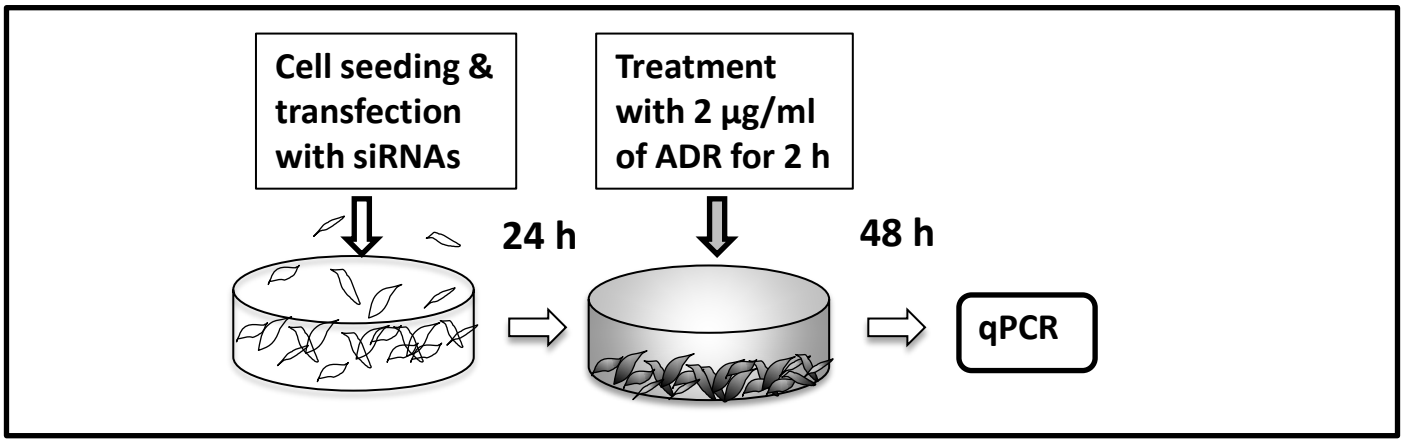

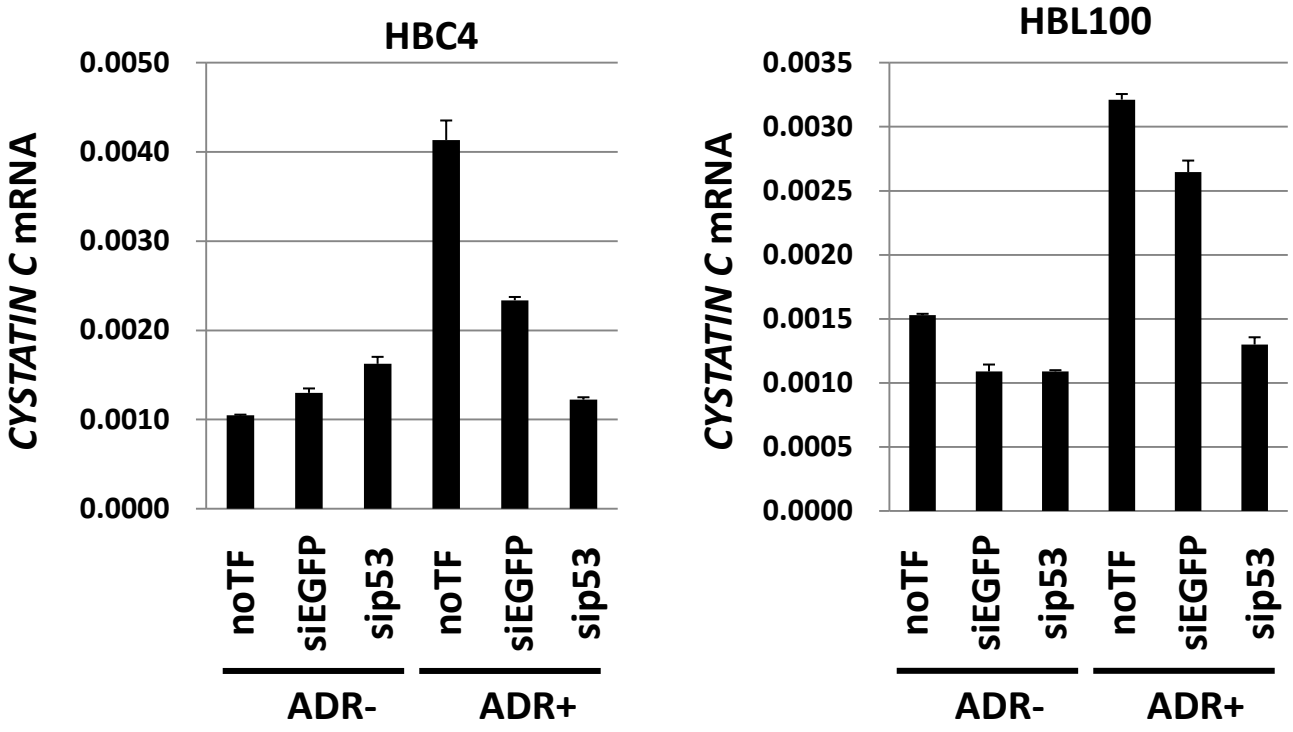

Figure 11. Induction of CYSTATIN C by DNA damage in breast cancer cells
HBC4 and HBL100 cells were transfected with sip53, 24 h prior to treatment with ADR. siEGFP and no transfection (noTF) were used as controls. At 48 h after 2 µg/ml of ADR treatment, total RNA were subjected to qPCR. *β-actin* was used for the normalization of expression levels. Error bars represent S.D. (n = 3).

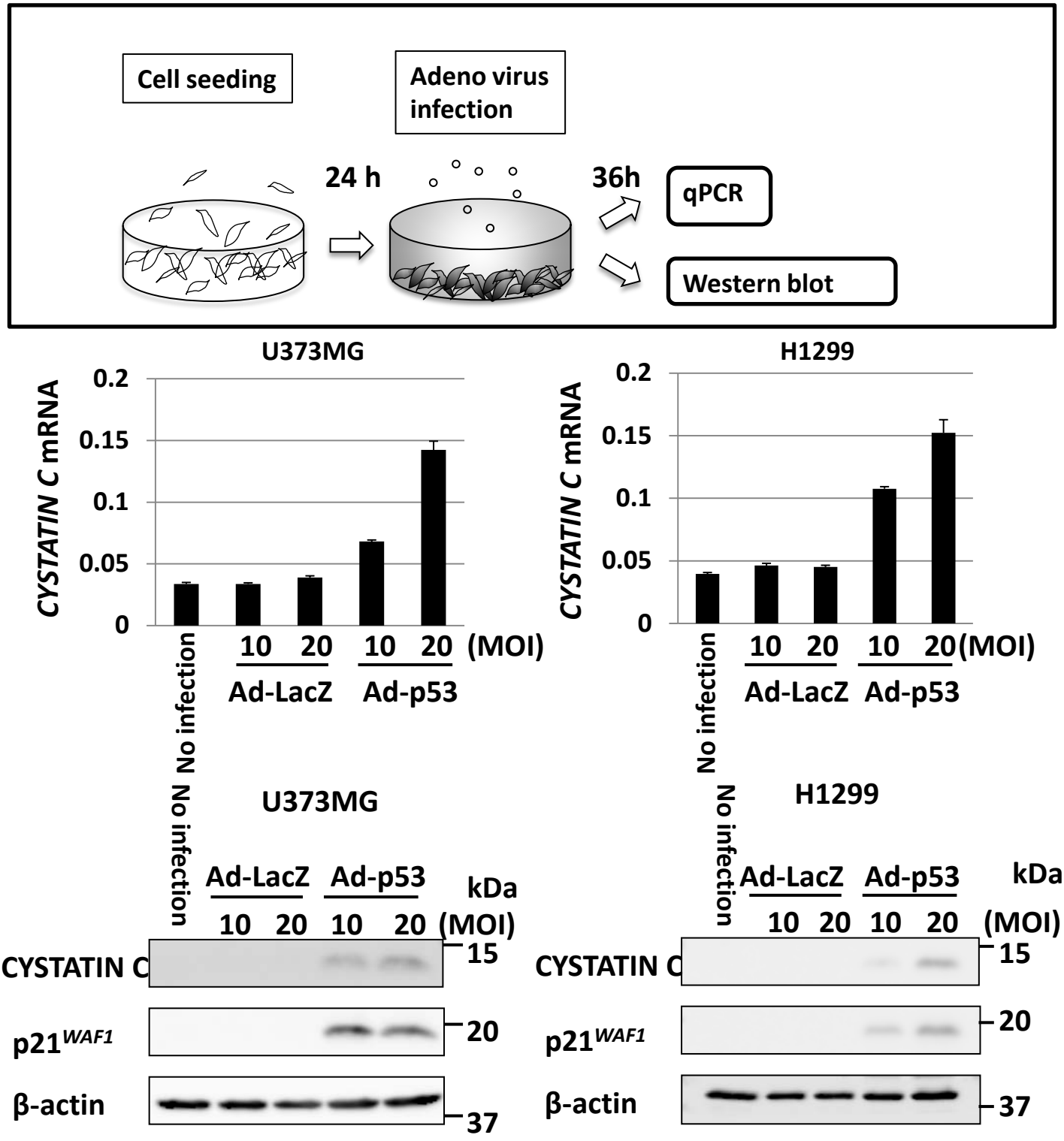

Figure 12. Induction of CYSTATIN C by p53.
(Upper) qPCR analysis of CYSTATIN C in U373MG and H1299 cells infected with Ad-p53)or Ad-LacZ at MOI of 10 or 20. *β-actin* was used for the normalization of expression levels. Error bars represent S.D. (n = 3). (Lower) U373MG cells were infected with Ad-p53 or Ad-LacZ at MOI of 10 or 20. At 36 h after treatment, whole cell extracts were subjected to immunoblotting with anti-CYSTATIN C, anti-p21, or anti-actin antibody

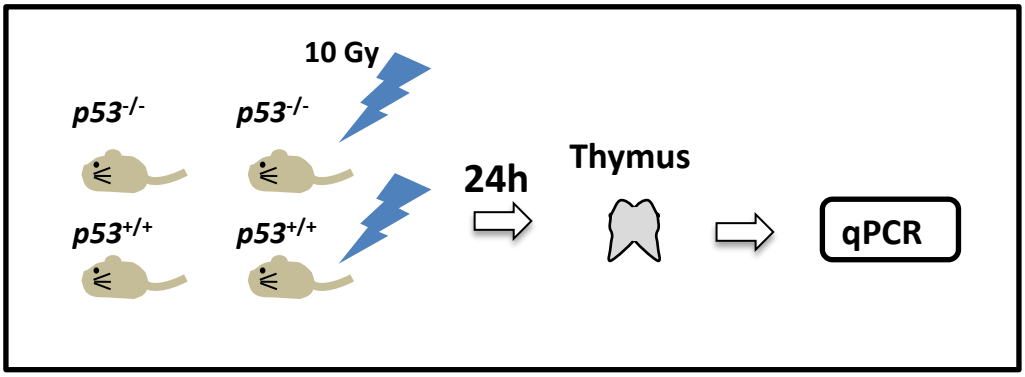

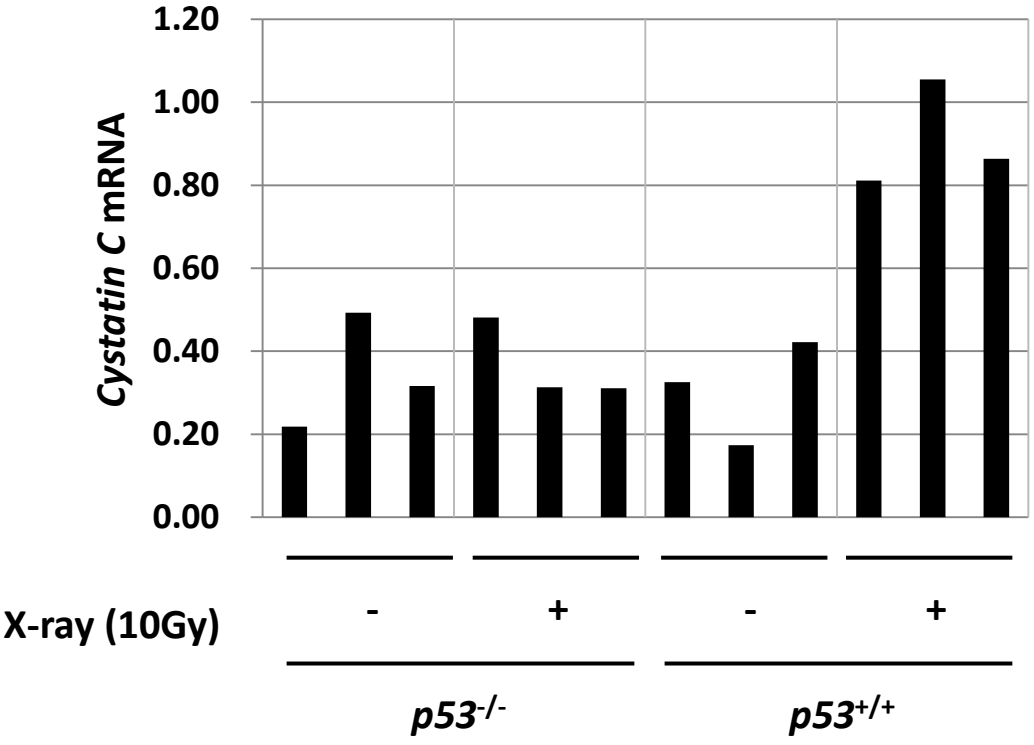

Figure 13. Induction of CYSTATIN C by DNA damage in mouse tissues
qPCR analysis of *cystatic C* expression in the thymus of X-ray-irradiated *p53*$^{-/-}$ or *p53*$^{+/+}$ mice (10 Gy) (n=3 per group). *β-actin* was used for the normalization of expression levels. Mice were sacrificed 24 h after irradiation with 10 Gy of X-ray.

Consensus	R R R C W W G Y Y Y R R R C W W G Y Y Y	
p53BS 1	A G G C A T G C T g G G G C g T G g T C	17/20
p53BS 2	c t G C A A G T C a G G A C A g G T T T	16/20
p53BS 1mut	A G G T A T T C T g G G G T g T T g T C	
p53BS 2mut	c t G T A A T T C a G G A T A g T T T T	

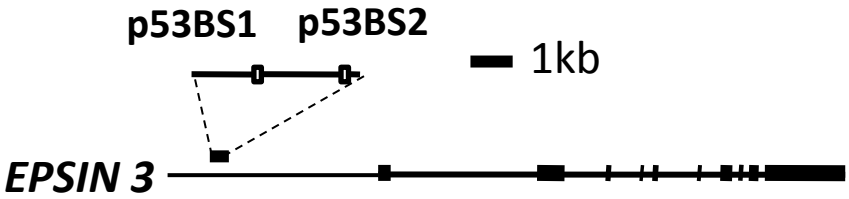

Consensus	R R R C W W G Y Y Y R R R C W W G Y Y Y	
p53BS	G A G C A T G C C T G A c C c T G C C T	18/20
p53BSmut	G A G T A T T C C T G A c T c T T C C T	

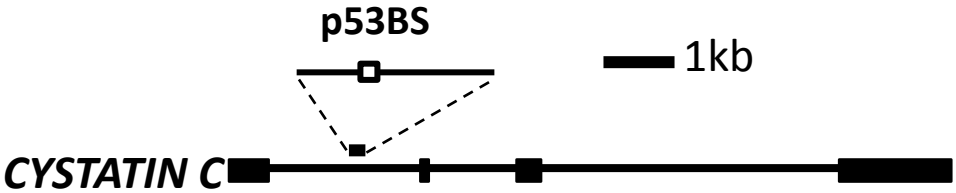

Figure 14. Genomic structure of *EPSIN 3* and *CYSTATIN C* gene.
The white boxes indicate the location of the potential p53-binding sequence (p53BS). Comparison of p53BS to the consensus p53-binding sequence. R, purine; W, A or T; Y, pyrimidine. Identical nucleotides to the consensus sequence are written in capital letters. The underlined cytosine and guanine were substituted for thymine to examine the specificity of the p53-binding sequence.

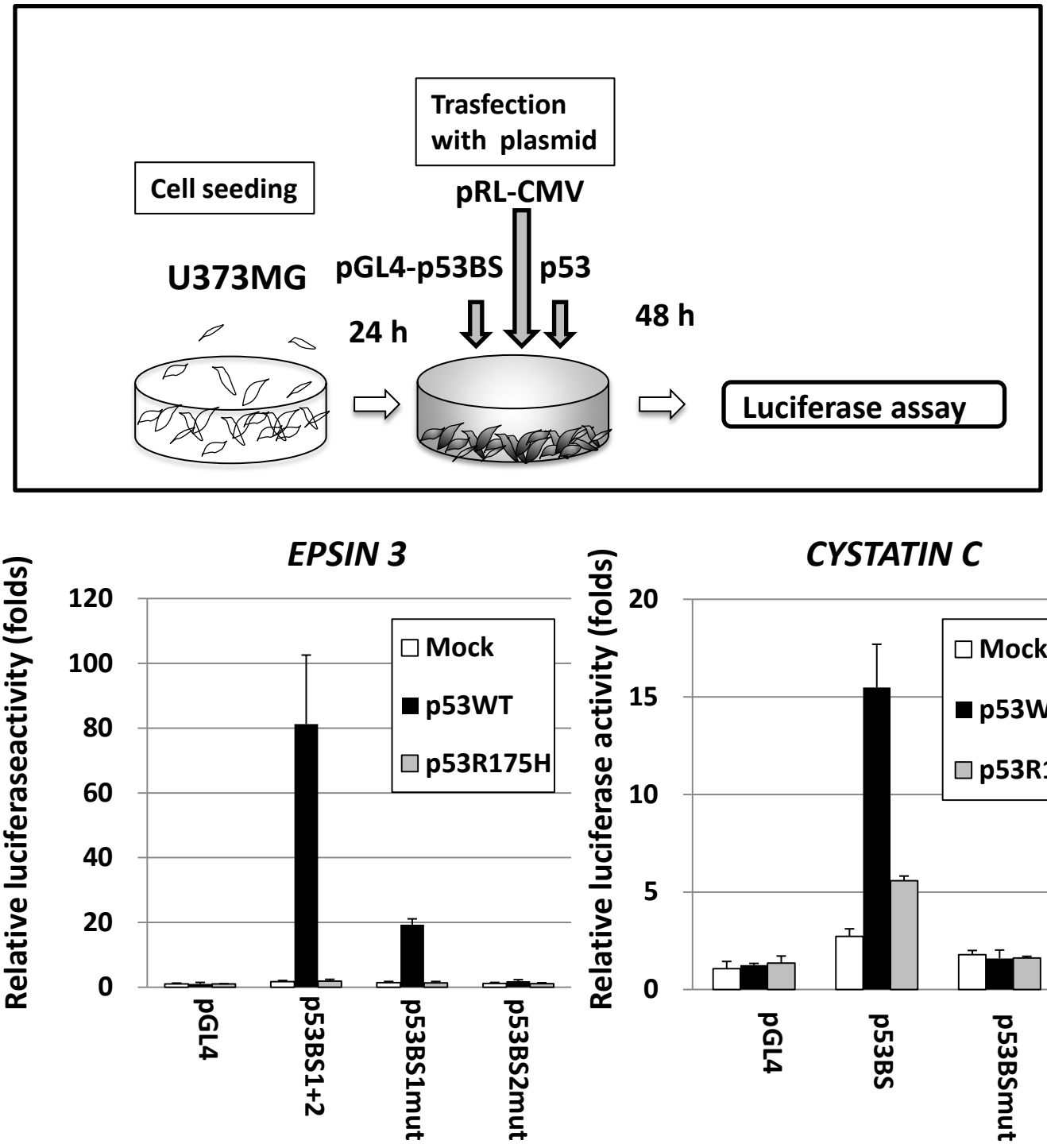

Figure15. p53 transactivates luciferase throμgh p53BSs

Results of luciferase assay of the genomic fragment containing p53BSs with or without substitutions at p53BSs. Luciferase activity is indicated relative to the activity of mock vector with S.D. (n = 3). Mutant p53 represents plasmid expressing p53 with a missense mutation (R175H).

Consensus	**R R R C W W G Y Y Y R R R C W W G Y Y Y**	
mp53BS	**G G A C c T G T g a A G A C T T G T g g**	**15/20**

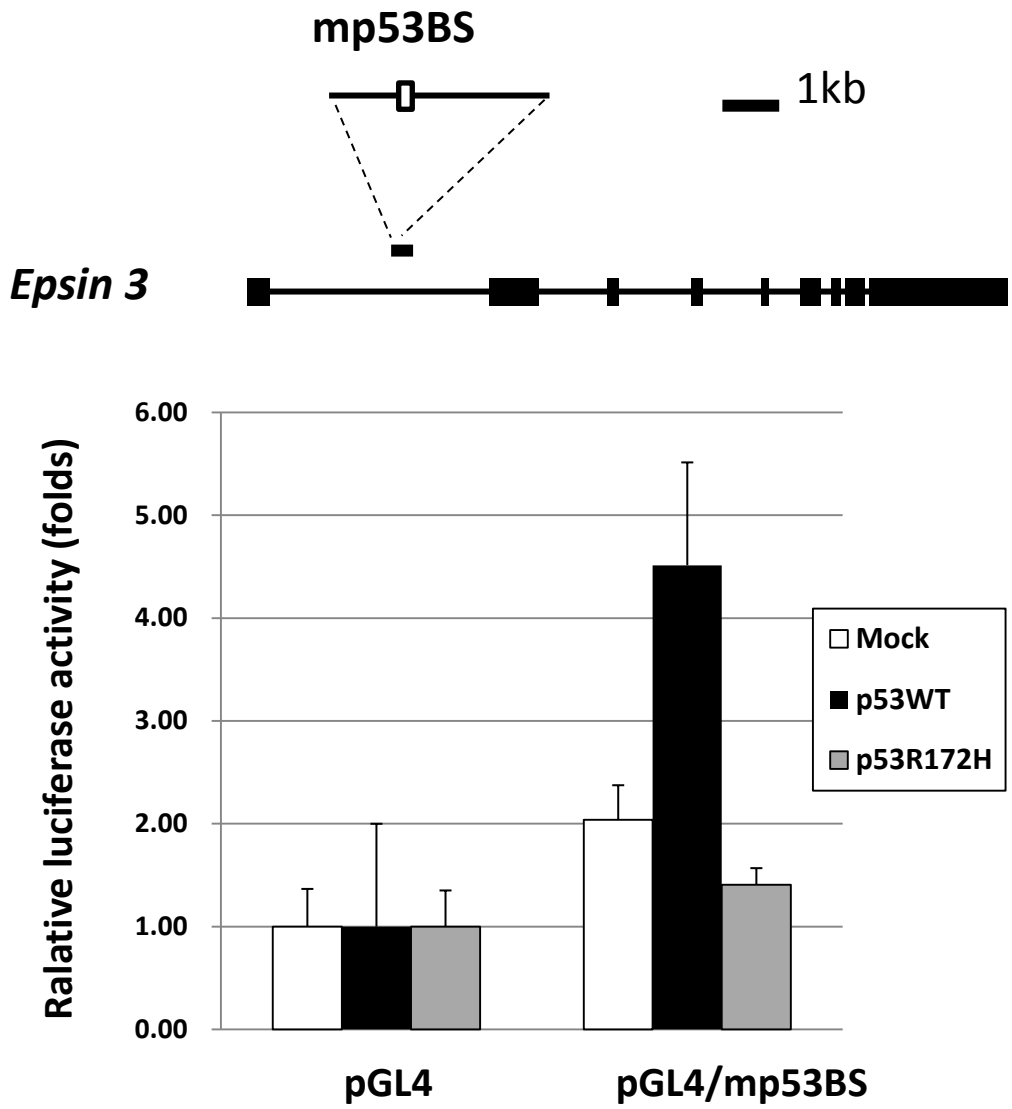

Figure 16. Genomic structure of mouse *Epsin 3* gene and the results of reporter assay
(A) The white boxes indicate the location of the potential p53-binding sequence (mp53BS). Comparison of mp53BS to the consensus p53-binding sequence. R, purine; W, A or T; Y, pyrimidine. Identical nucleotides to the consensus sequence are written in capital letters. (B) Results of luciferase assay of the genomic fragment containing. Luciferase activity is indicated relative to the activity of mock vector with S.D. (n = 3).

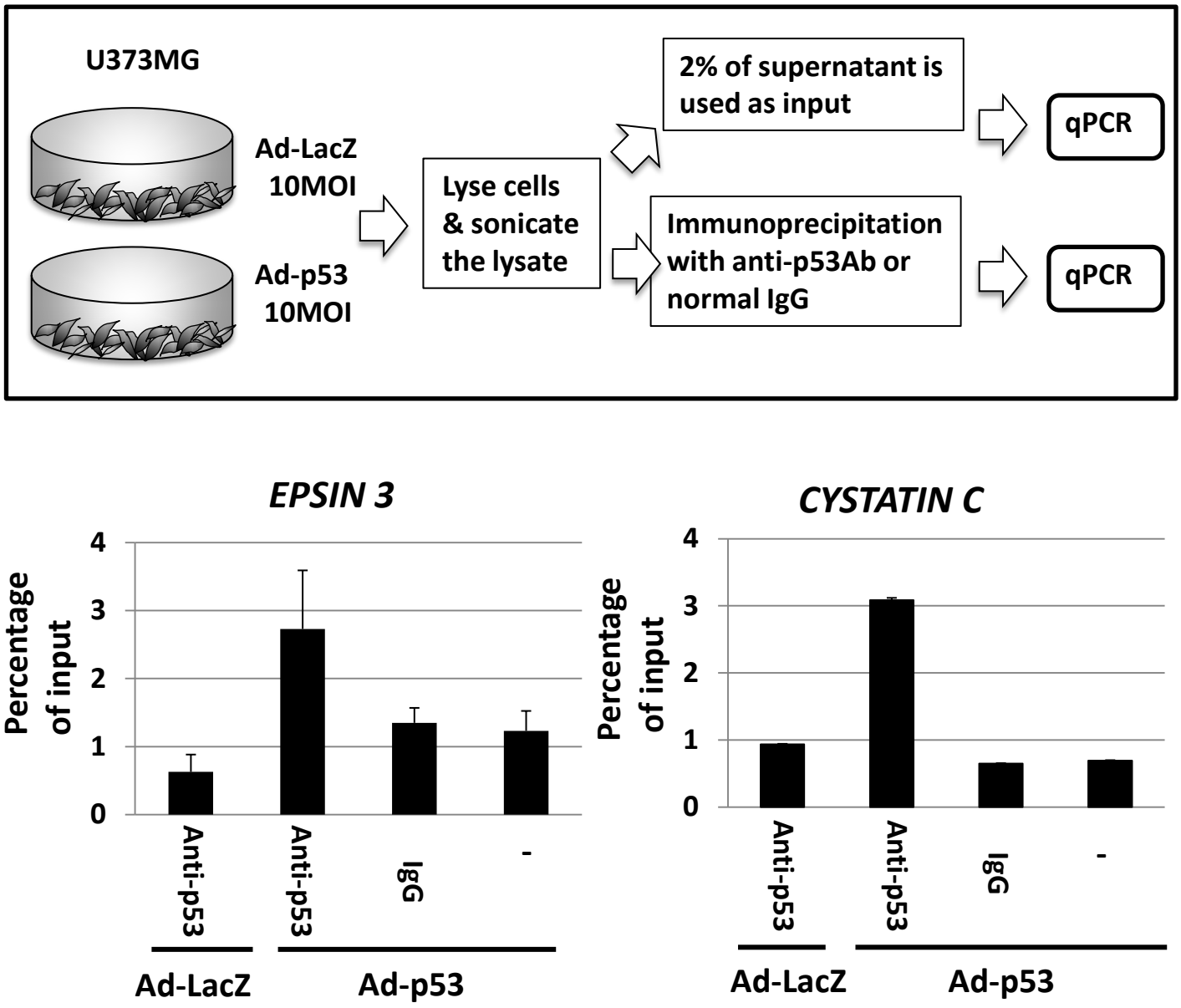

Figure 17. p53 directly binds to p53 binding sequences of *EPSIN 3* and *CYSTATIN C*
ChIP assay was performed using U373MG cells that were infected at an MOI of 10 with Ad-p53 (lane 2-4) or Ad-LacZ (lane 1). DNA-protein complexes were immunoprecipitated with an anti-p53 antibody (lane 1 and 2) followed by qPCR analysis. Input chromatin represents a small portion (2%) of the sonicated chromatin before immunoprecipitation. Immunoprecipitates with an anti-IgG antibody (lane 3) or in the absence of an antibody (lane 4) were used as negative controls. Error bars represent S.D. (n = 3).

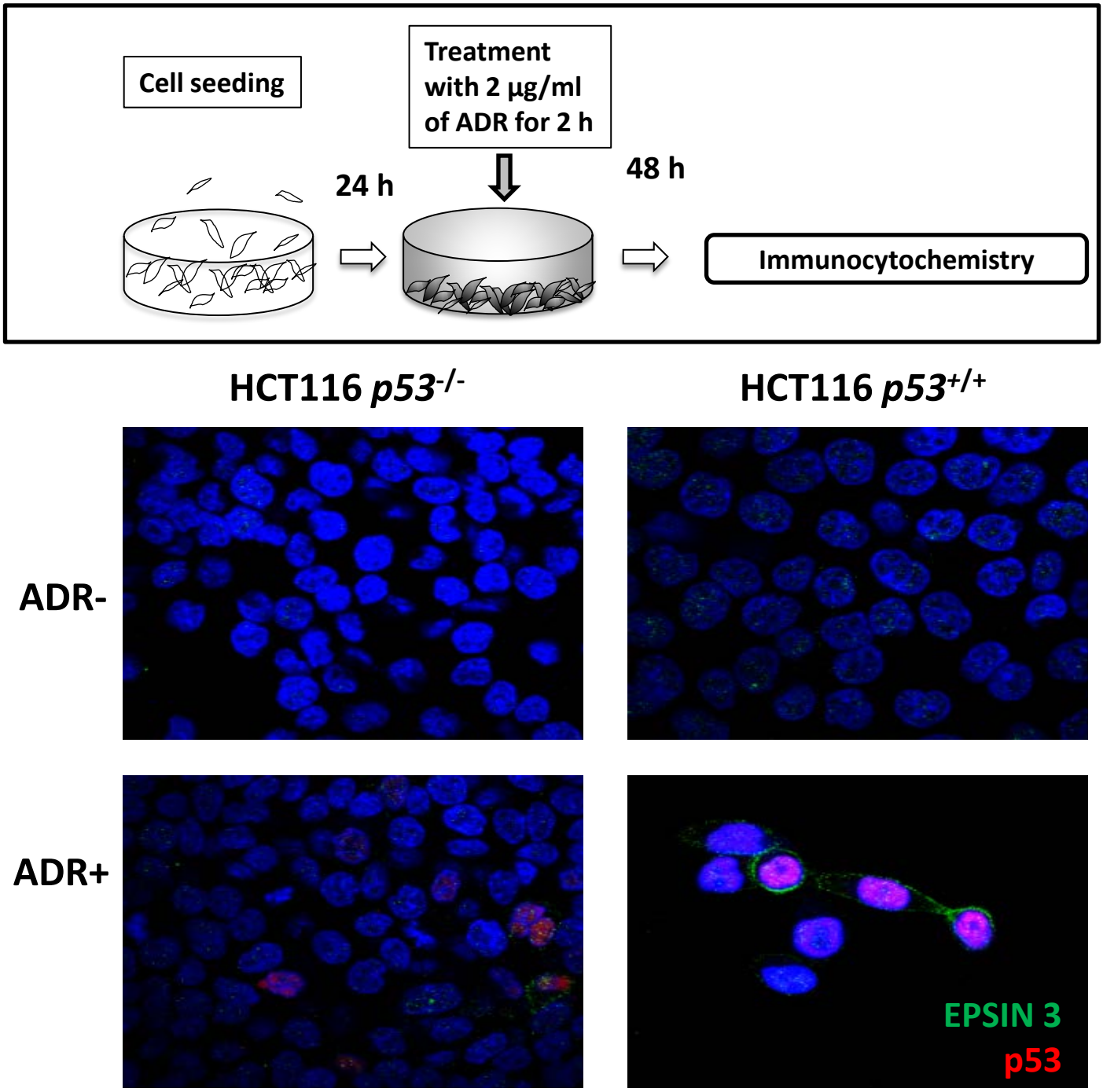

Figure 18. Endogenous EPSIN 3 is localized in inner surface of plasma membrane. After 2 µg/ml of ADR treatment for 2 h or no treatment, HCT116 *p53*$^{-/-}$ or *p53*$^{+/+}$ cells were incubated for 48 h. Adherent cells were fixed with 4% paraformaldehyde in PBS and permeabilized with 0.2% Triton X-100 in PBS for 5 min at room temperature. EPSIN 3 (green) and p53 (red) were visualized using specific primary antibodies and fluorescein-conjµgated 2nd antibodies. Nucleus was stained with DAPI (blue).

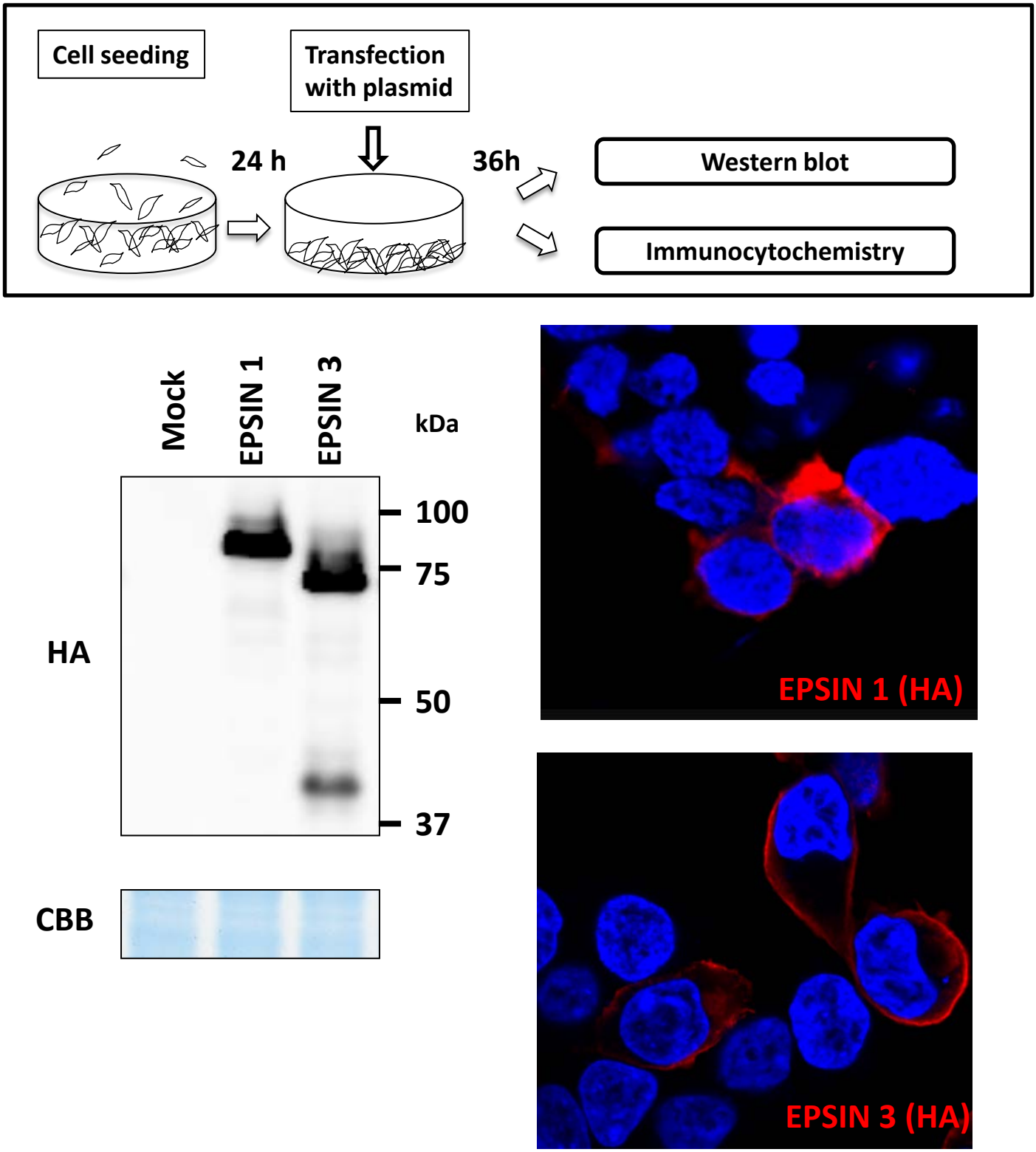

Figure 19. Exogenous epsin1 and 3 localized in inner surface of plasma membrane. Thirty-six hours after transfection with HA-tagged-EPSIN 3 expression vector, HA-tagged –epsin1 expression vector, or mock vector, HEK293T cells were collected and the whole cell extracts were subjected to westernblotting and immunocytochemistry analysis using anti-HA antibody.

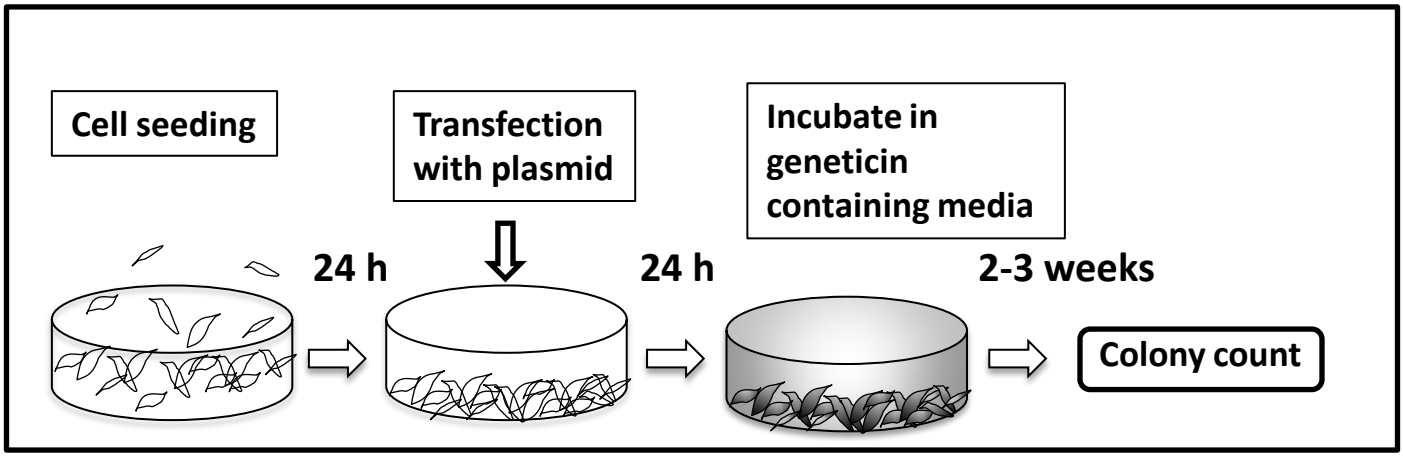

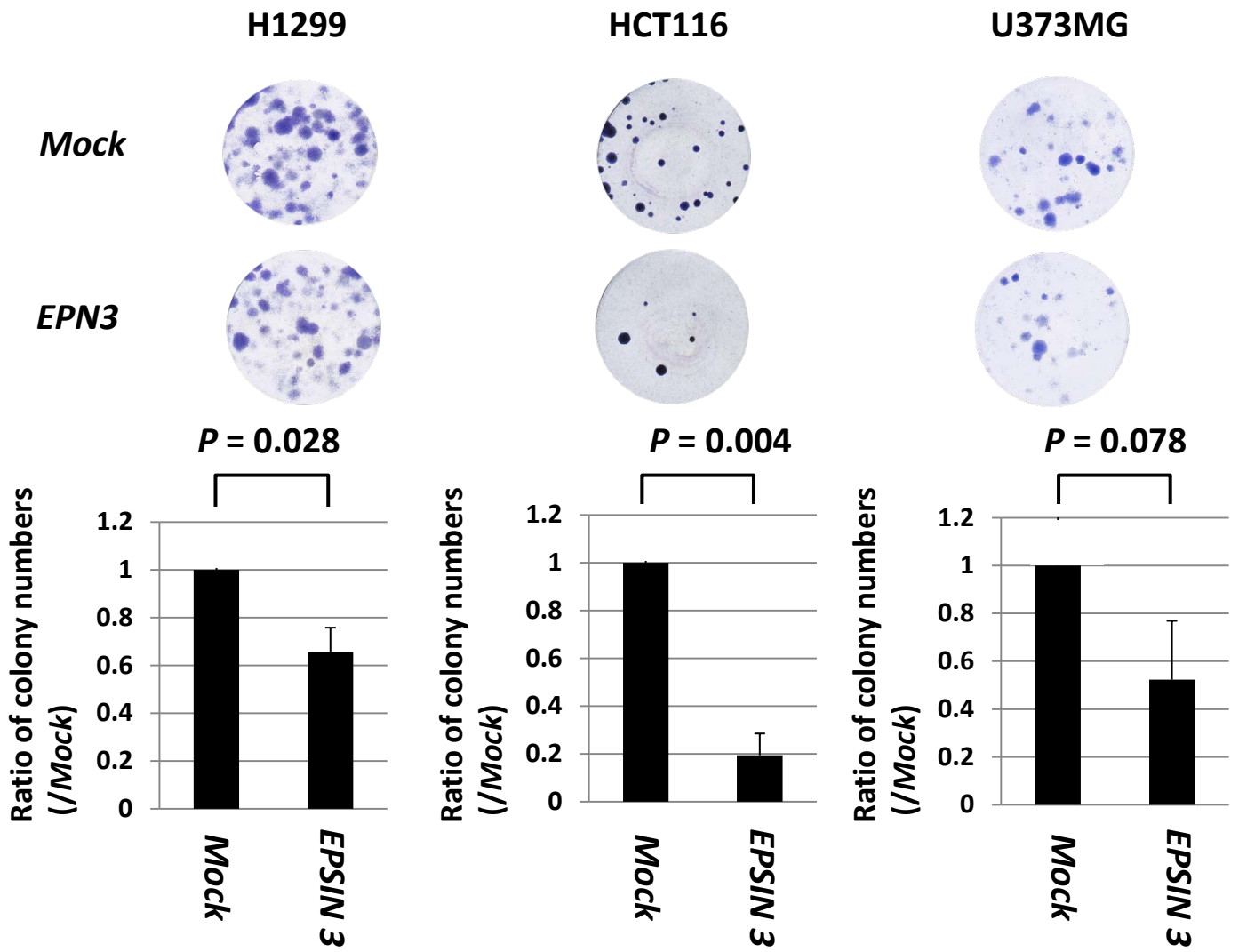

Figure. 20. Ectopically expressed EPSIN 3 suppressed cancer cell growth
H1299, HCT116 and U373MG cells transfected with EPSIN 3 expressing plasmid or mock vector were cultured in the media containing 0.8, 0.5 and 0.5 mg/ml of geneticin , respectively, for 2-3 weeks. Error bars represent S.D. (n = 3). P- value was calculated by Student's t-test.

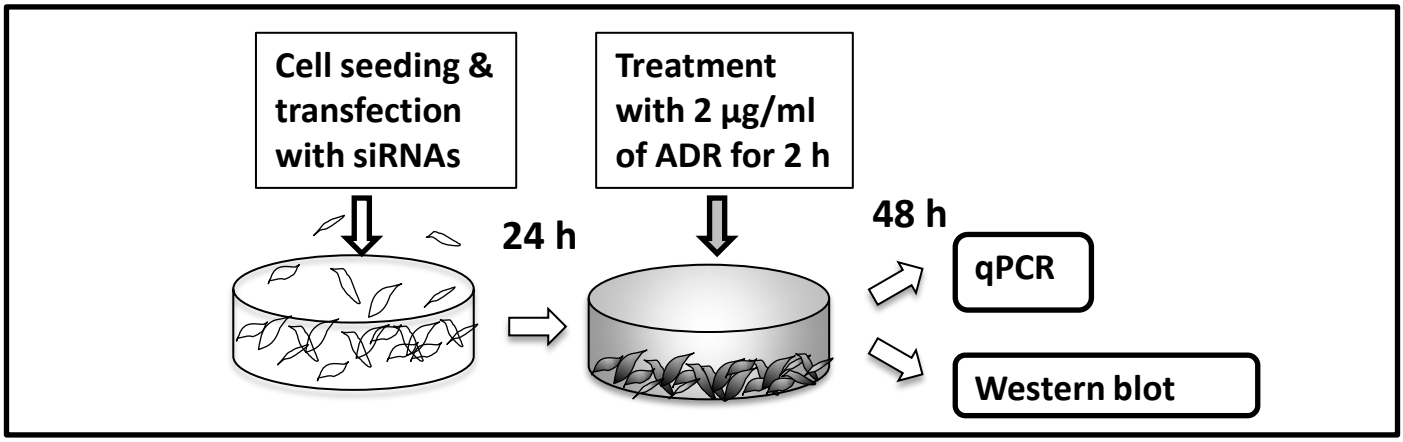

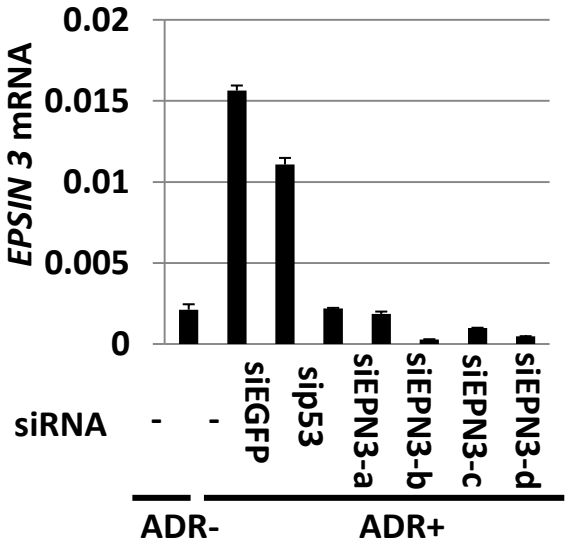

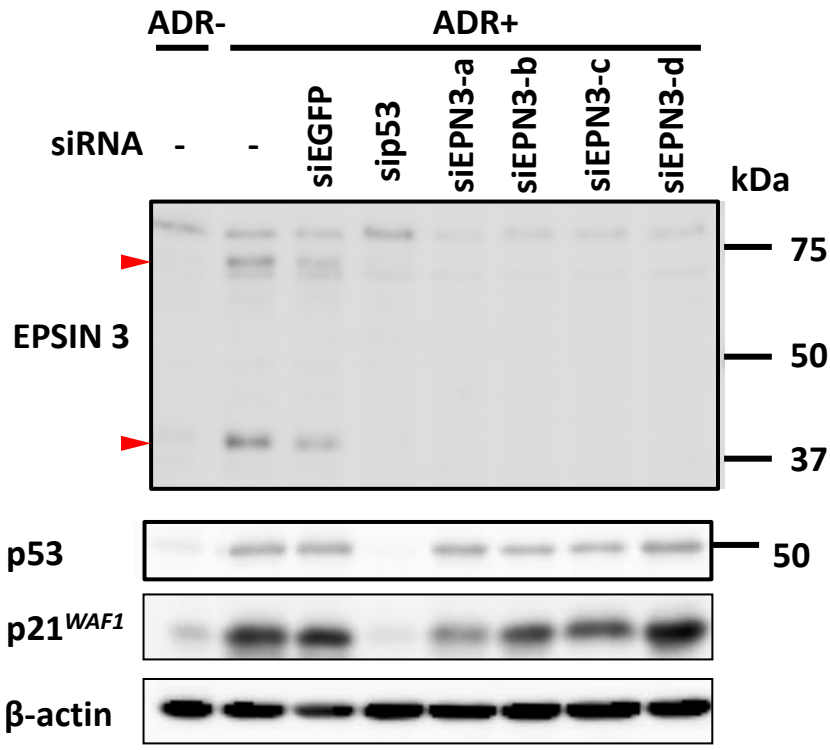

Figure 21. Knockdown of EPSIN 3 expression by siRNA.
We designed four small interference RNAs (siRNAs): siIEPN3-a-d. HCT116 cells were transfected with each siRNA, 24 h prior to treatment with ADR. siEGFP was used as a control. At 48 h after treatment, total RNA and whole cell extracts were subjected to qPCR and Western blot analysis, respectively. Red arrows indicate the protein bands of EPSIN 3. β-actin was used for normalization of expression levels in qRT-PCR analysis. Error bars represent S.D. (n = 2).

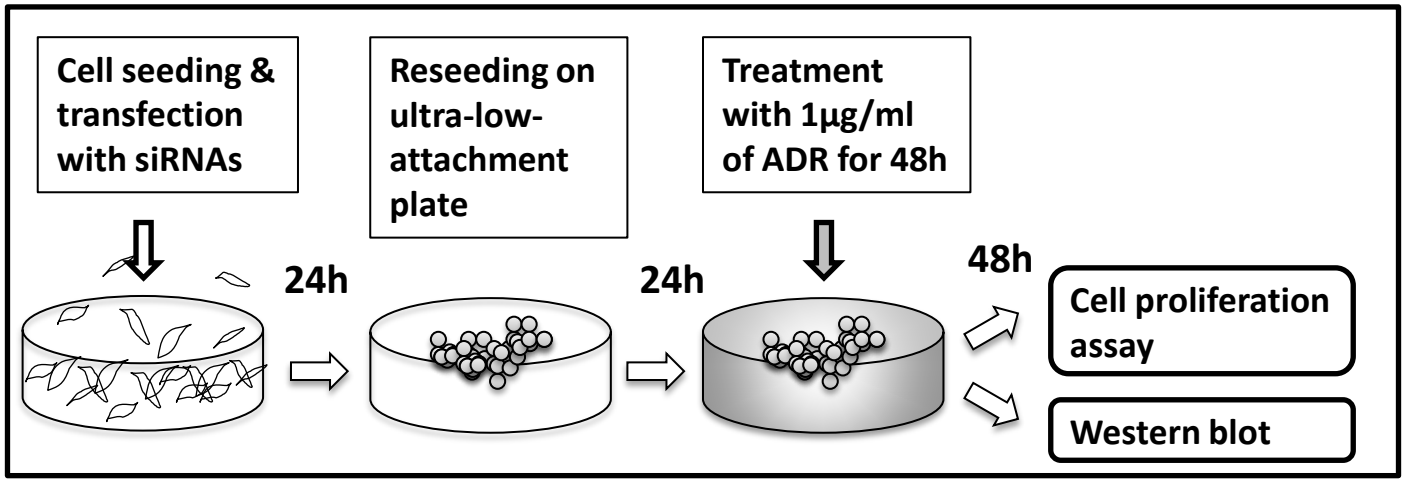

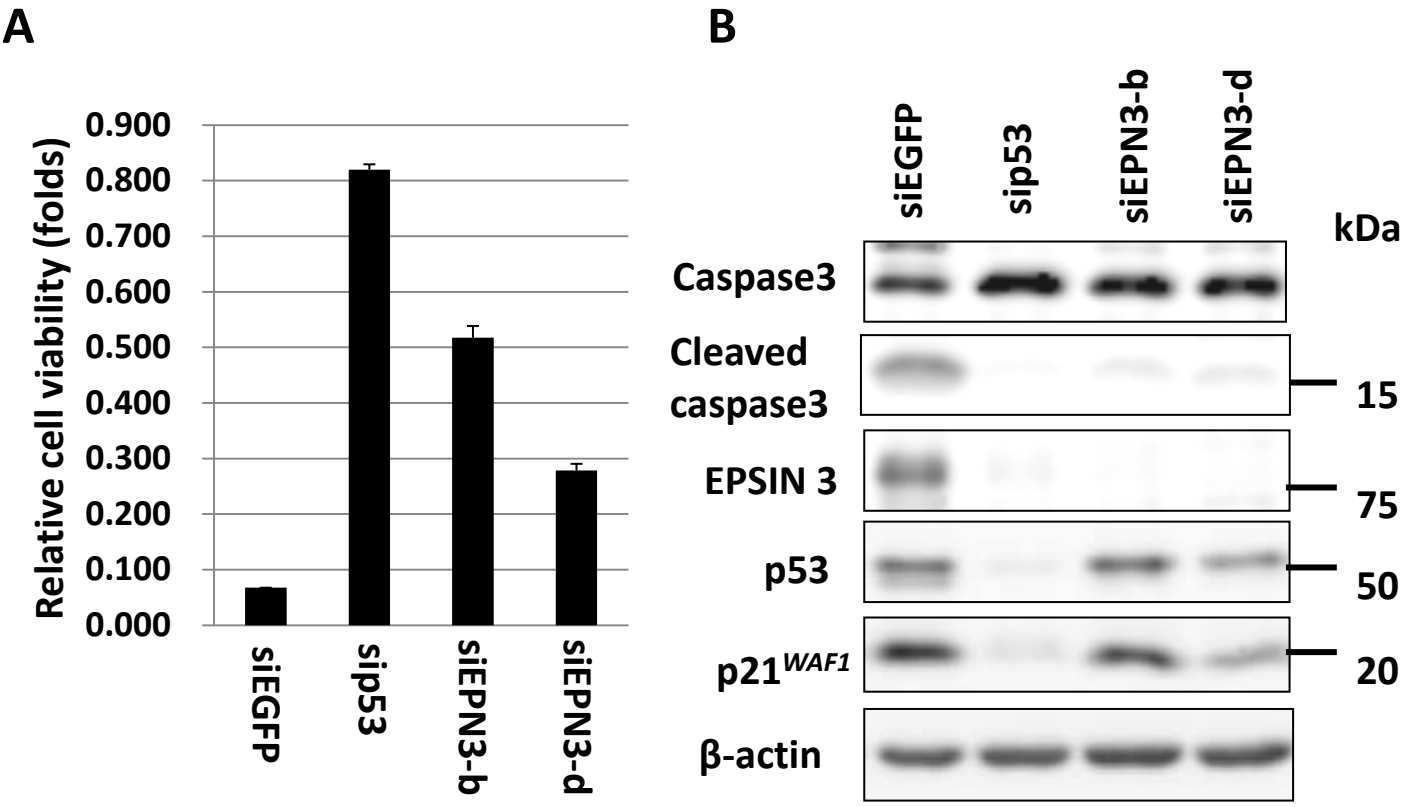

Figure 22. p53-EPSIN 3 regulates cell proliferation and apoptosis.
At 24 h after transfection of each siRNA, HCT116 cells were seeded and cultured on ultra-low attachment plates. At 24h after plating, HCT116 cells were treated with 1 μg/ml ADR for 48 h and subjected to (A) cell proliferation analysis. Relative cell viability was calculated by dividing the absorbance of ADR-treated cells by that of untreated cells. Error bars represent S.D. (n = 3). (B) Western blot analysis was performed using HCT116 cells treated as the same as above. siRNA against *EGFP* was used as control.

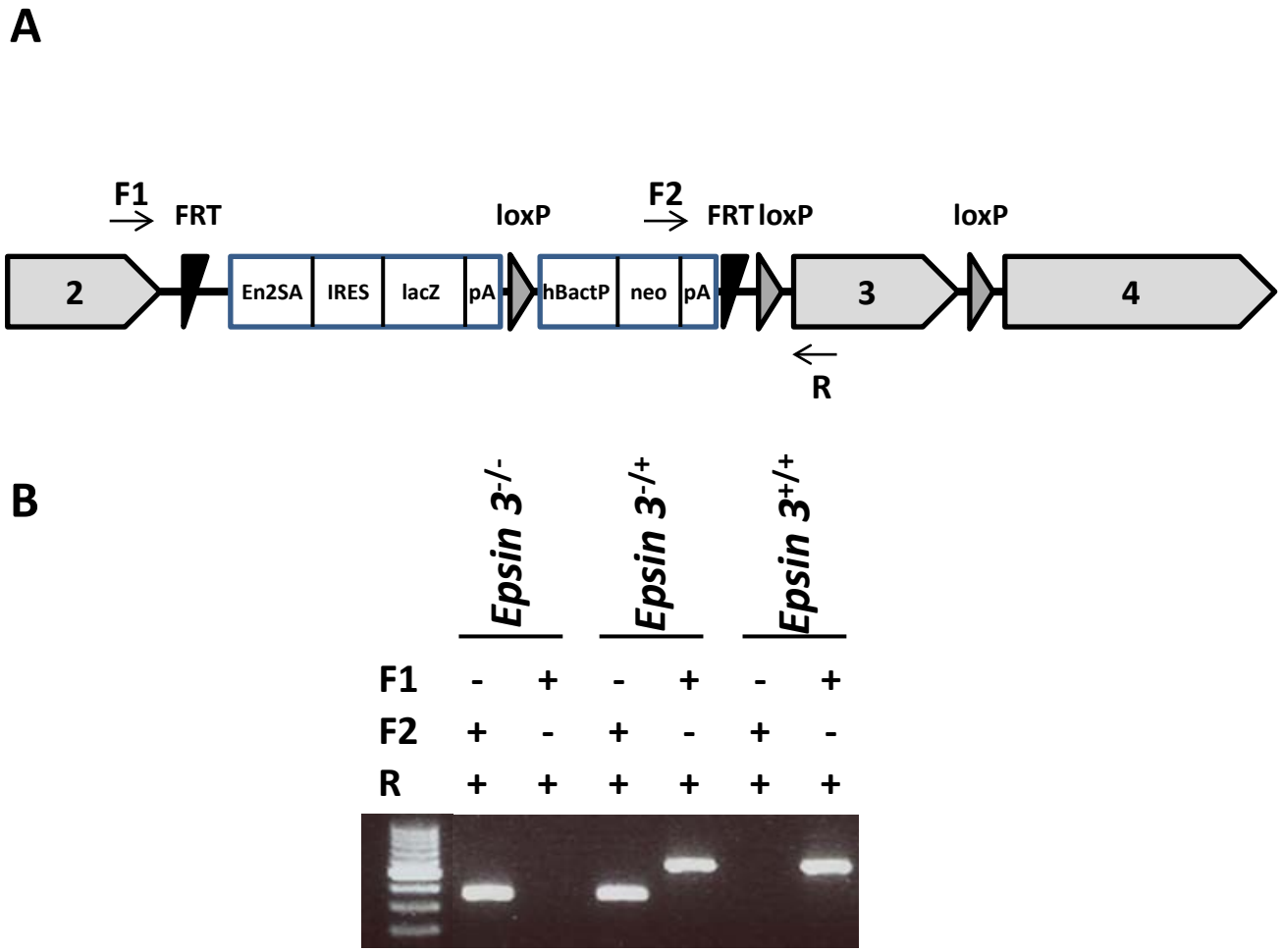

Figure 23. Schematic of knockout vector design and PCR for mouse genotyping. (A) Numbered boxes refer to *Epsin 3* exons. Arrows over and under DNA sequence indicate locations of primer for genotyping. (B) Result of PCR for mouse genotyping. The 100bp ladder size marker was run in lane 1. Predicted sizes of PCR product from F1 and R for wild type allele is 398bps, and F2 and R for knockout allele is 621bps.

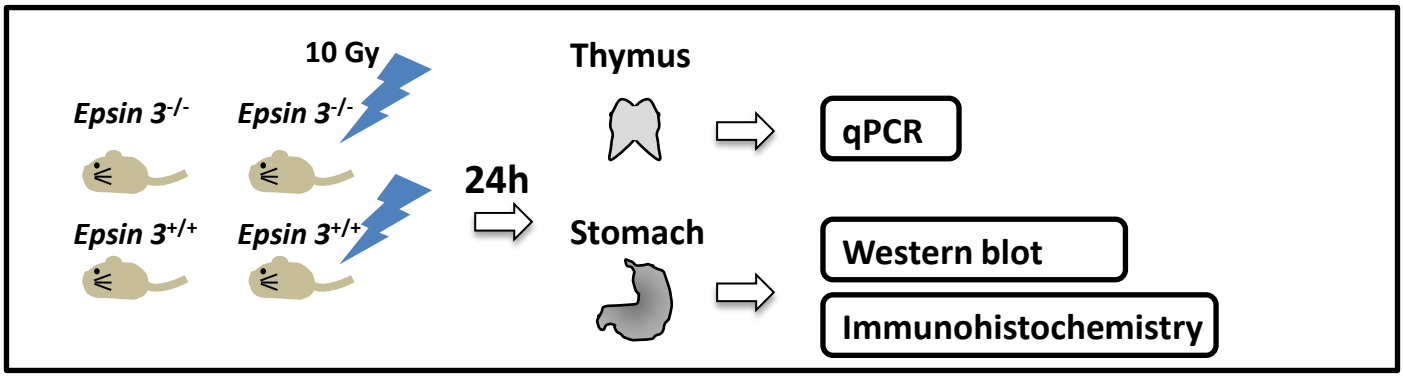

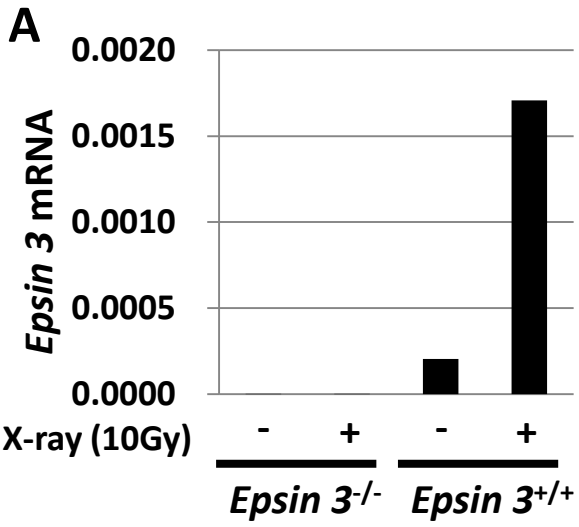

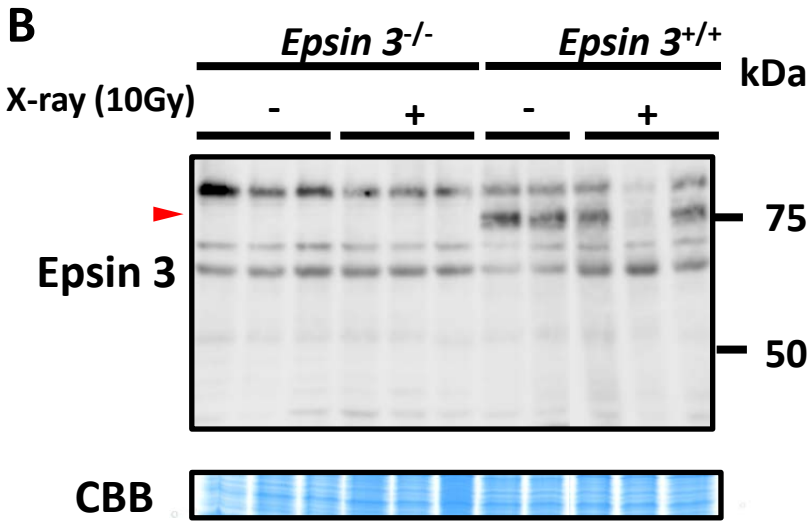

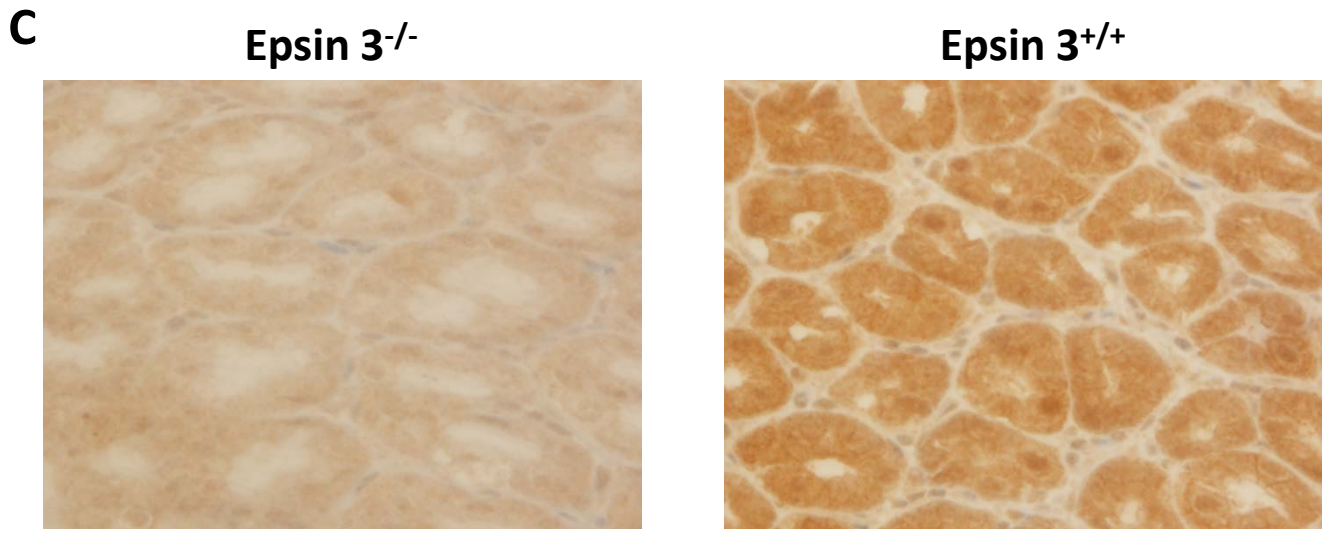

Figure 24. Confirmation of Epsin 3 knockout.
(A) qPCR analysis of *Epsin 3* expression in the thymus of X-ray-irradiated *Epsin 3*$^{-/-}$ or *Epsin 3* $^{+/+}$ mice (10 Gy) (n=1 per group). *β-actin* was used for the normalization of expression levels. (B) Western blot analysis of Epsin 3 protein expression in the stomach of X-ray-irradiated *Epsin 3*$^{-/-}$ or *Epsin 3* $^{+/+}$ mice (10 Gy) (n=2-3per group). Red arrow indicates the protein band of Epsin 3. CBB staning was used for the loading control. (C) Immunohistochemistry analysis of Epsin 3 protein expression in the stomach of X-ray-irradiated *Epsin 3*$^{-/-}$ or *Epsin 3* $^{+/+}$ mice (10 Gy). All mice were sacrificed 24 h after irradiation.

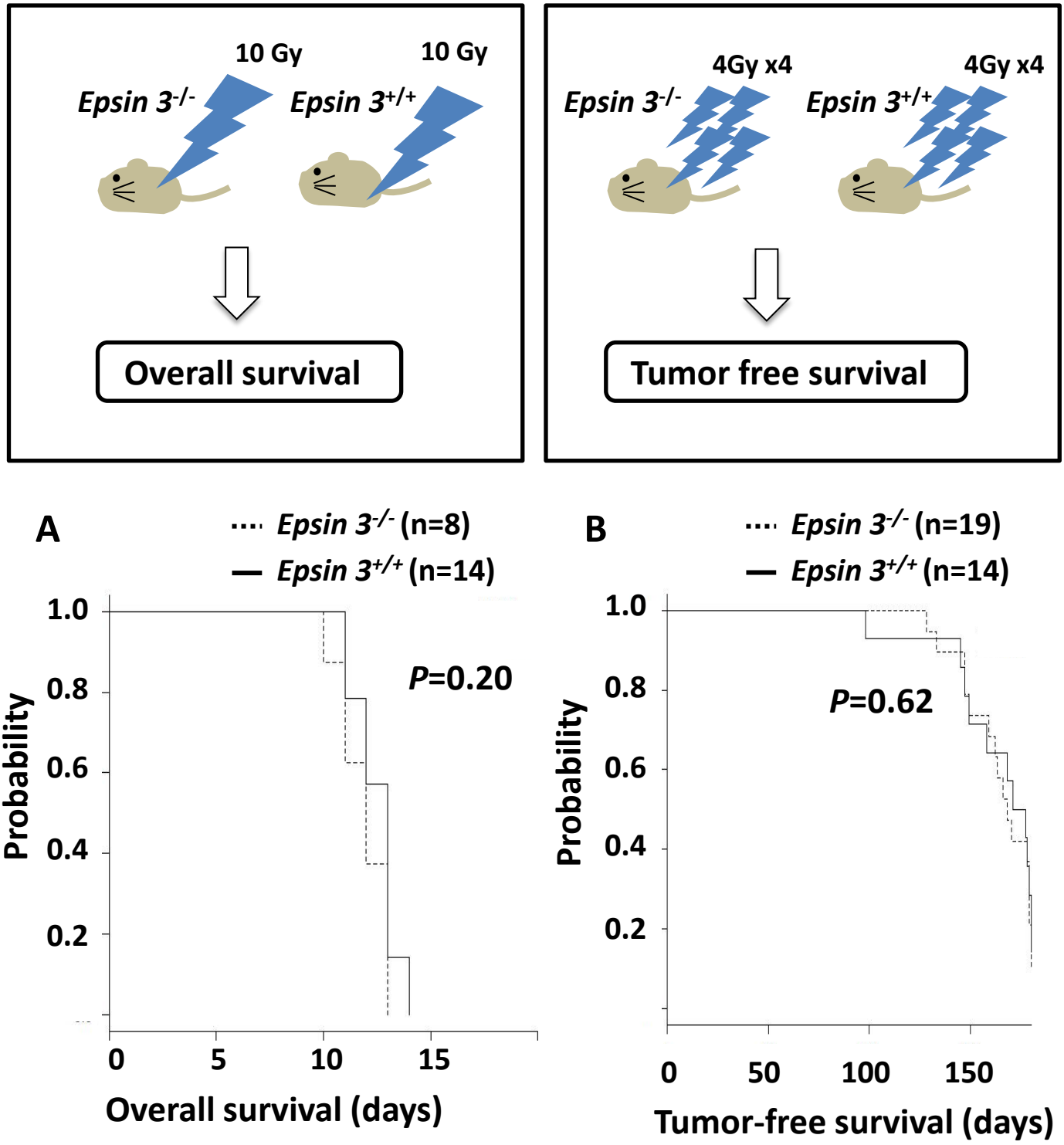

Figure 25. Survival and tumor development analysis of *Epsin 3* wild-type and deficient mice.

(A)Overall survival and (B) tumor-free survival curves of *Epsin* $3^{-/-}$ (dashed lines) and *Epsin* $3^{+/+}$ (dashed lines) mice were plotted using Kaplan-Meier method. P-values were calculated by log-rank test. Mice were irradiated 10Gy at day 0 and 4 Gy of X-ray weekly for 4 weeks.

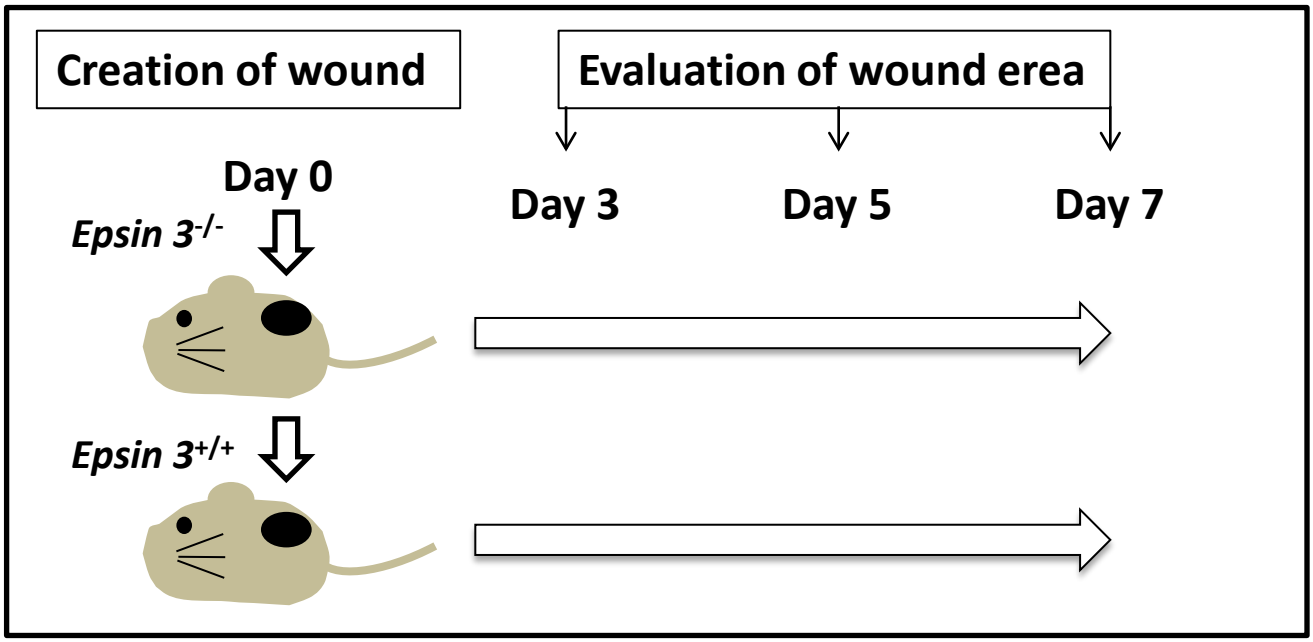

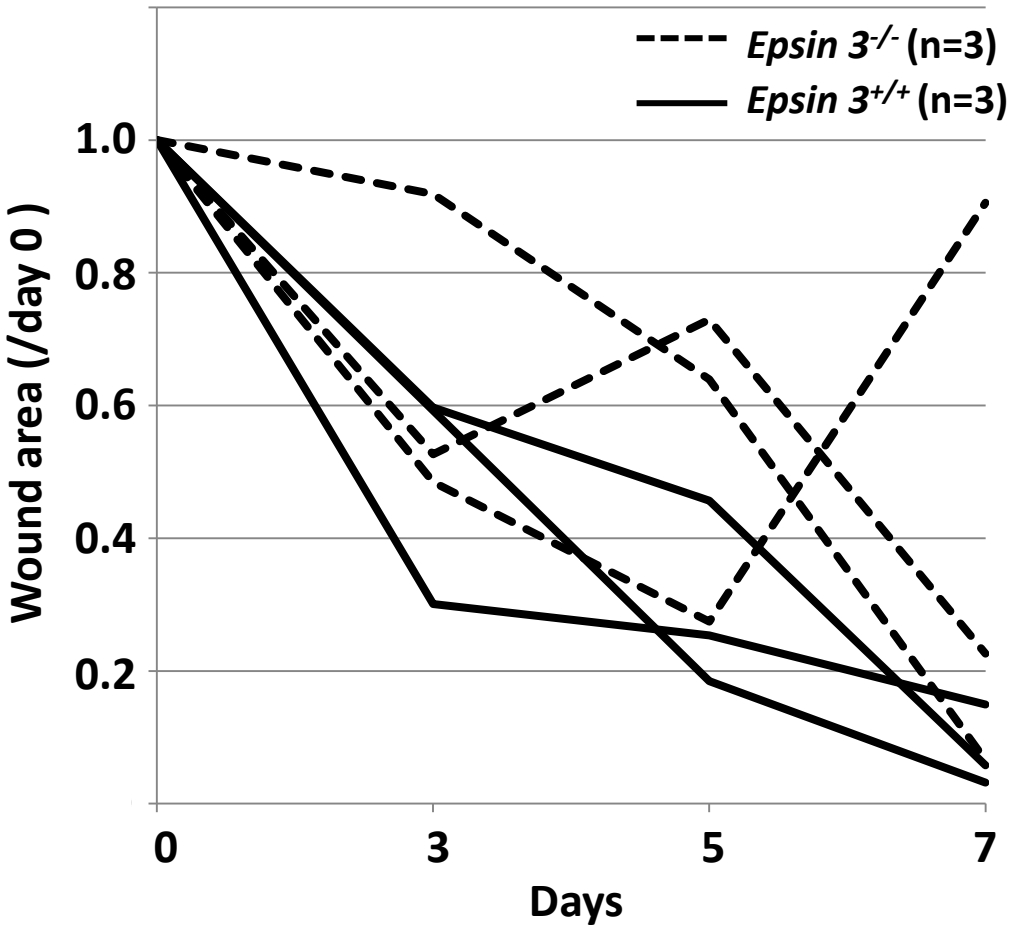

Figure 26. Wound healing experiment of *Epsin 3* wild-type and deficient mice.
Sequential change of the area of wounds created on the dorsa of *Epsin 3*$^{-/-}$ (dashed lines) and *Epsin 3*$^{+/+}$ (dashed lines). The area at each time-point was divided by the area at day 0.

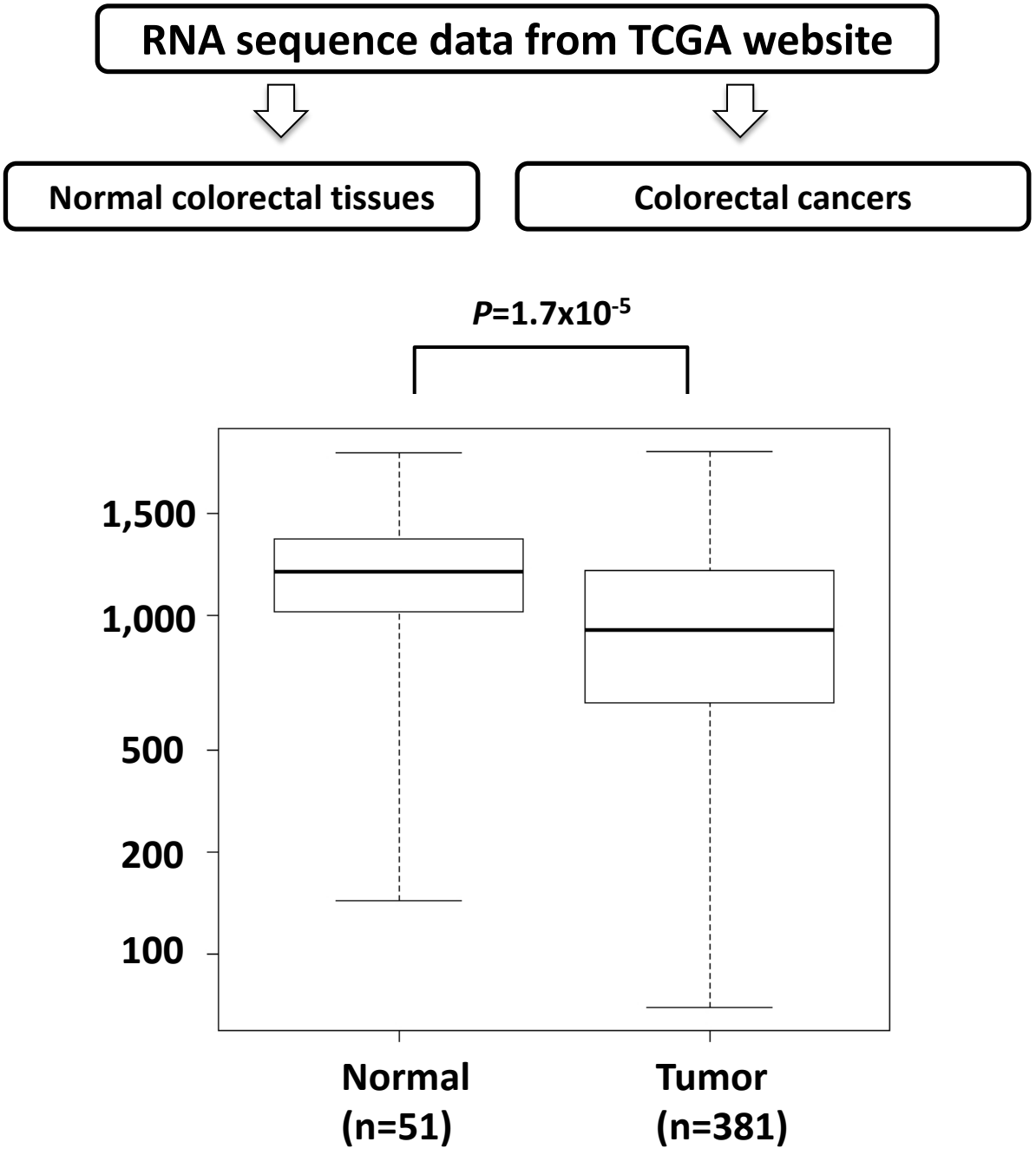

Figure 27. Relation of *EPSIN 3* expression in cancer tissues.
Using the data of RNA sequence in human colorectal cancer tissues obtained from The Cancer Genome Association (TCGA) database, gene expression analysis was performed. Box-plot indicates *EPSIN 3* expression in colorectal tissues. The vertical axis indicates the normalized expression level of *EPSIN 3*, top bar represents maximum observation, lower bar represents minimum observation, top of the box is upper or third quartile, bottom of the box is lower or first quartile, middle bar is median value. P value was calculated by Mann-Whitney U test.

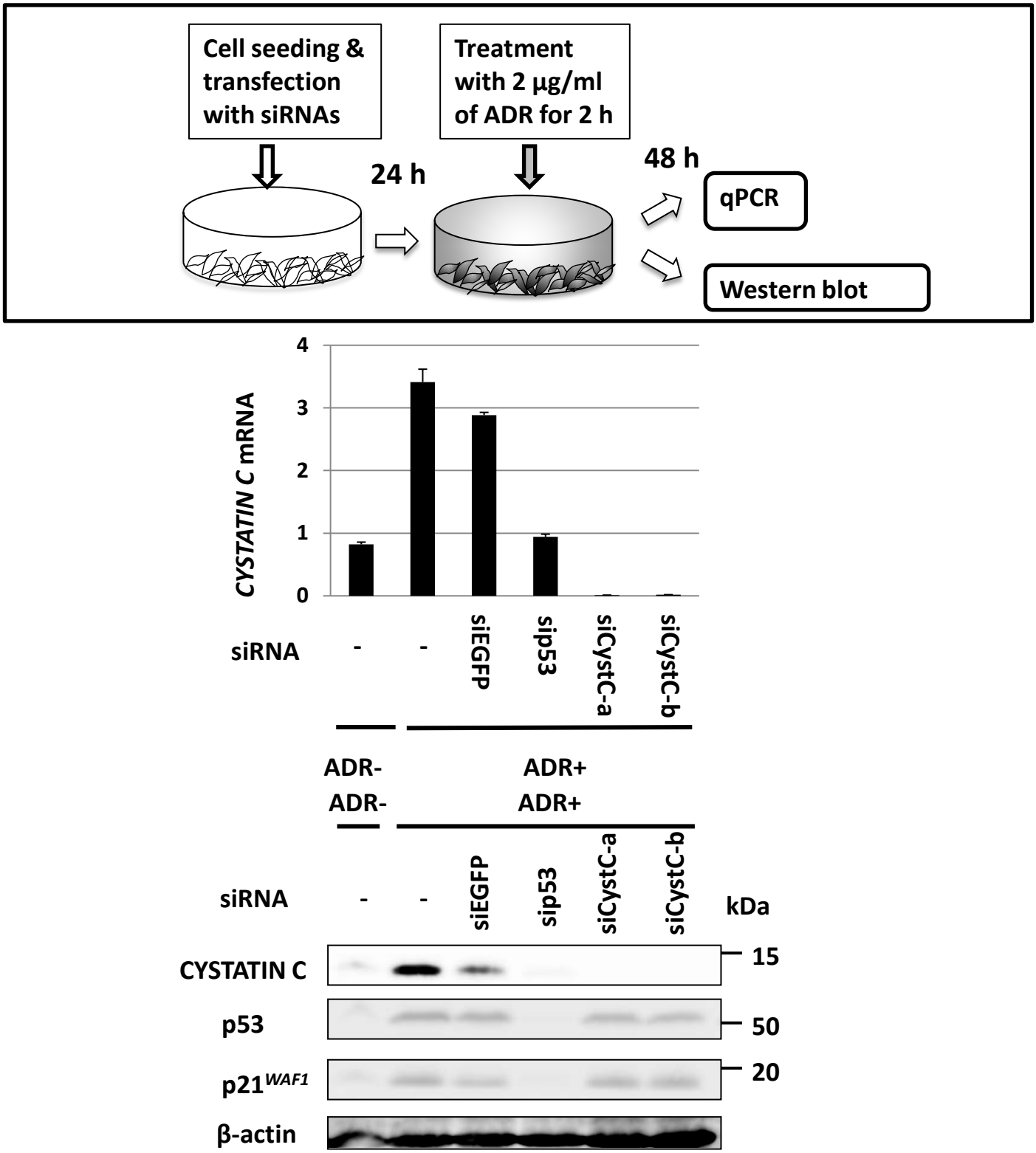

Figure 28. Knockdown of CYSTATIN C expression by siRNA.
HCT116 cells were transfected with small interference RNAs (siRNAs) against CYSTATIN C: siCystC-a and -b, 24 h prior to treatment with ADR. siEGFP was used as a control. At 48 h after treatment, total RNA and whole cell extracts were subjected to qPCR and immunoblot analysis, respectively. β-actin was used for normalization of expression levels in qRT-PCR analysis. Error bars represent S.D. (n = 3).

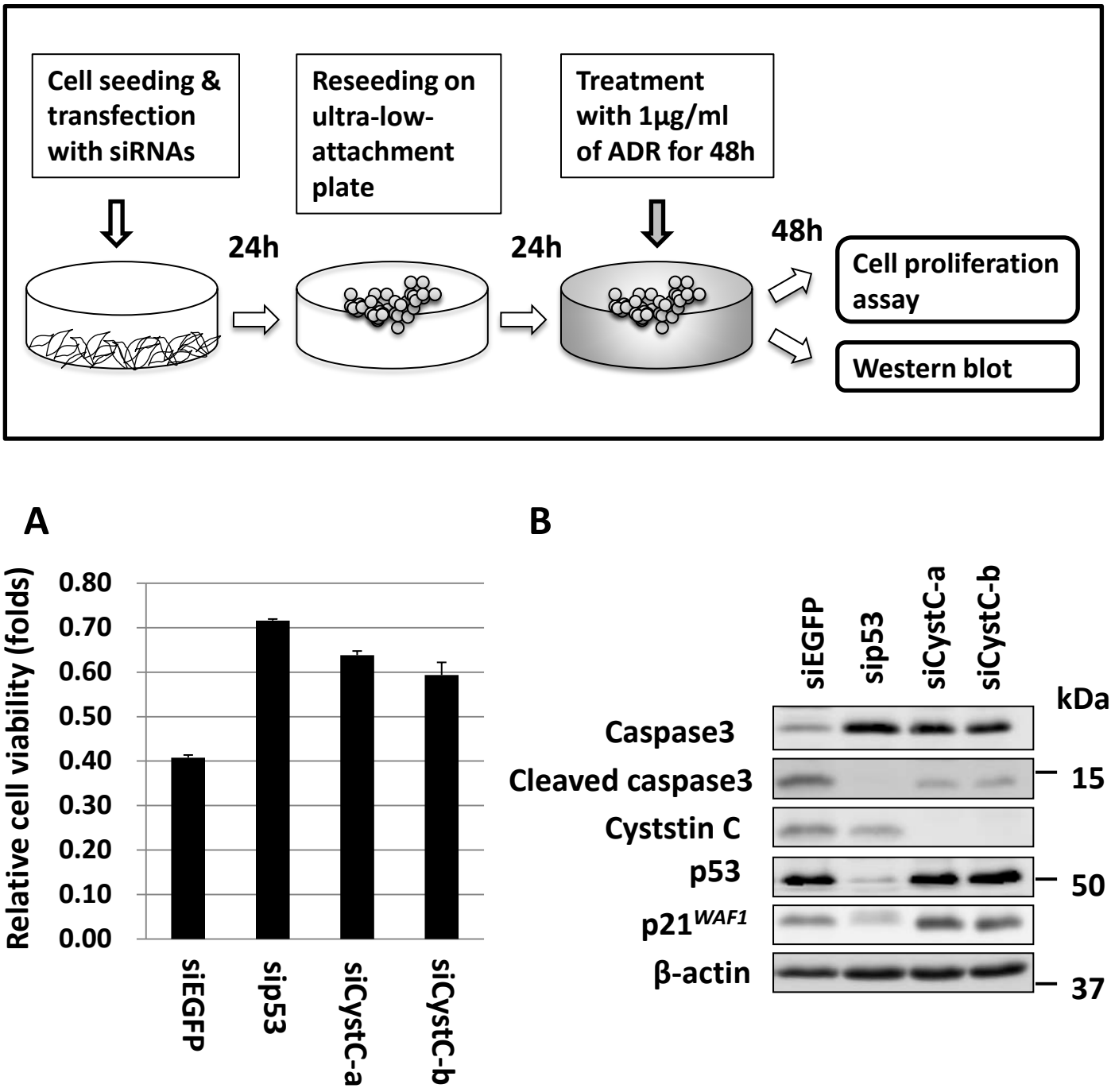

Figure 29. p53-CYSTATIN C regulates cell proliferation and apoptosis
At 24 h after transfection of each siRNA, HCT116 cells were seeded and cultured on ultra-low attachment plates. At 24h after plating, HCT116 cells were treated with 1 μg/ml ADR for 48 h and subjected to (A) cell proliferation analysis. Relative cell viability was calculated by dividing the absorbance of ADR-treated cells by that of untreated cells. Error bars represent S.D. (n = 3). (B) Western blot analysis was performed using HCT116 cells treated as the same as above. siRNA against *EGFP* was used as control.

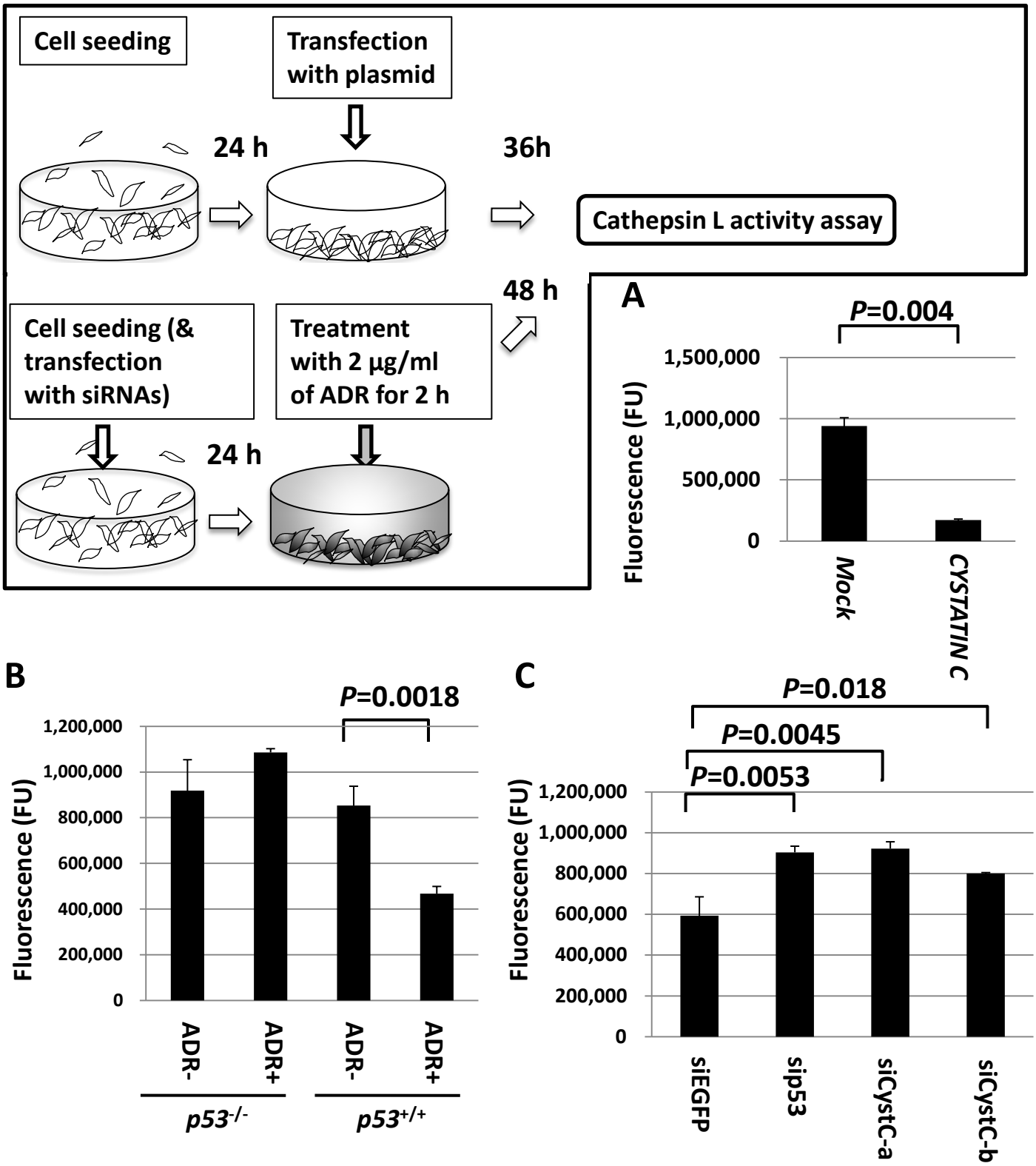

Figure 30. Cathepsin L activity was regulated by p53-CYSTATIN C pathway.
(A) HEK293T cells were transfected with CYSTATIN C expression plasmid or mock plasmid, (B) HCT116 *p53*$^{+/+}$ or HCT116 *p53*$^{-/-}$ cells were treated with 2 μg/ml ADR for 2 h, or (C) HCT116 *p53*$^{+/+}$ transfected with each siRNA were treated with 2 μg/ml ADR for 2 h. Cathepsin L activity was measured at 36 h after transfection or 48 h after ADR treatment. Error bars represent S.D. (n = 3). P- value was calculated by Student's t-test.

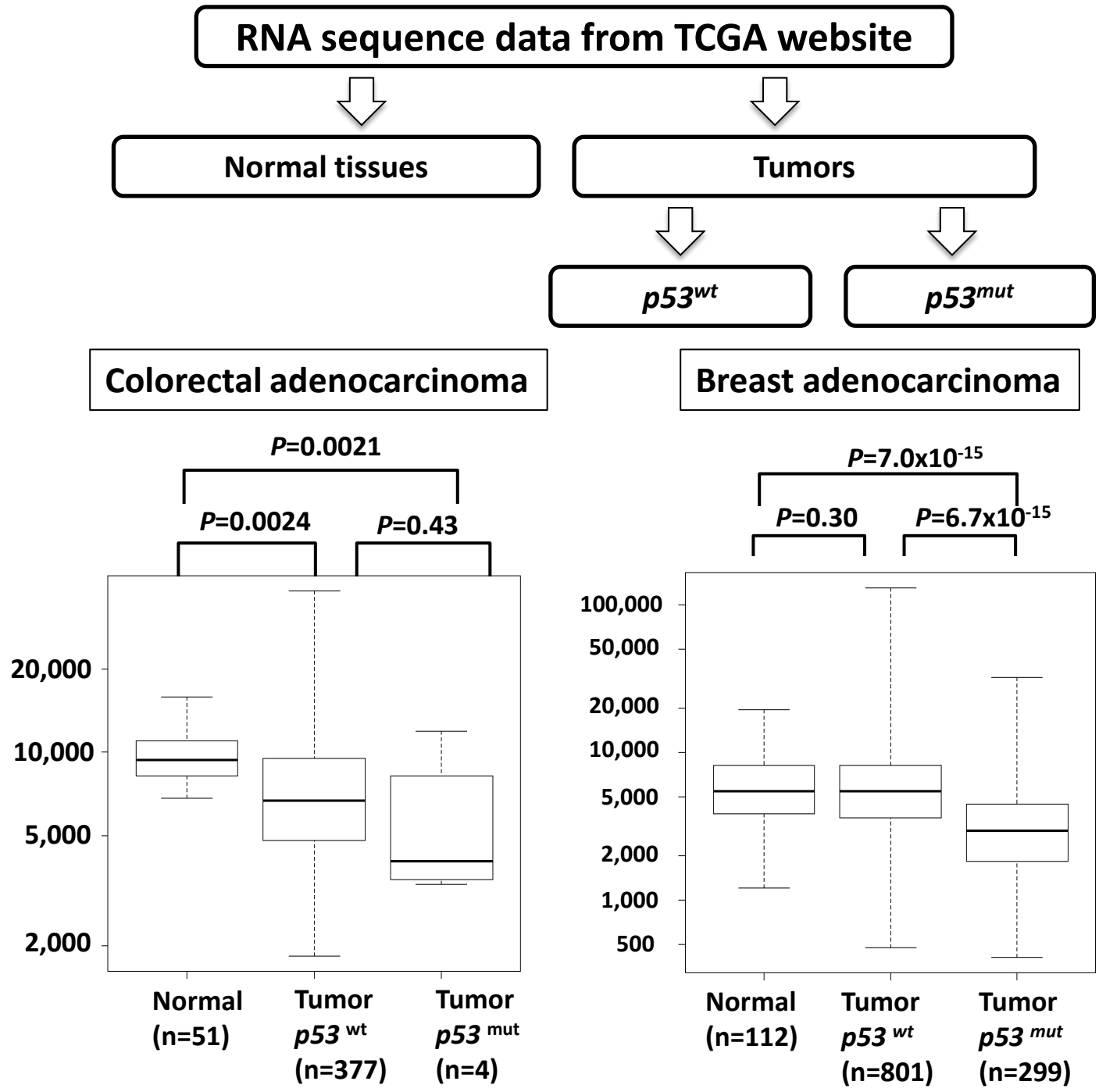

Figure 31. Relation of *CYSTATIN C* expression and *p53* status in cancer tissues.
Using the sequence data of DNA and RNA in human cancer tissues obtained from TCGA database, gene expression analysis was performed. Box-plots indicate *CYSTATIN C* expression in (left) colorectal adenocarcinoma or (right) breast adenocarcinoma tissues. The vertical axis indicates the normalized expression level of *CYSTATIN C*, top bar represents maximum observation, lower bar represents minimum observation, top of the box is upper or third quartile, bottom of the box is lower or first quartile, middle bar is median value. P value was calculated by Mann-Whitney U test.

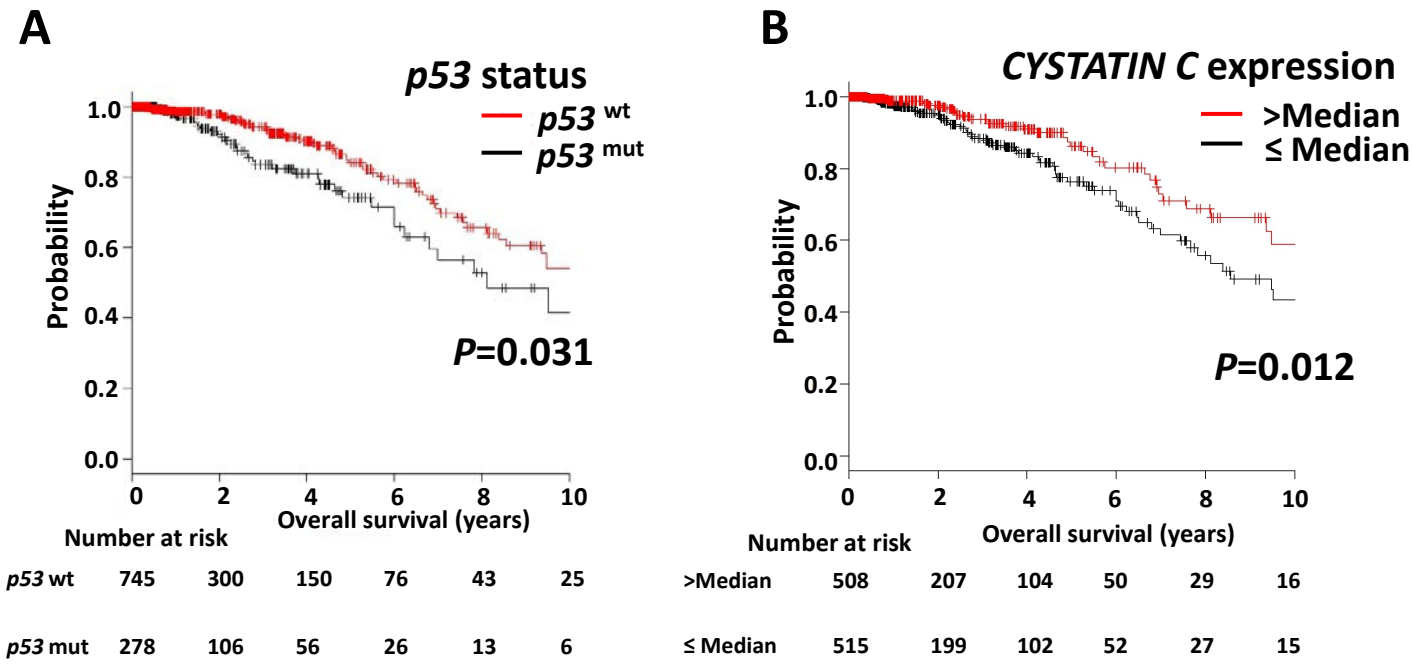

Figure 32. Prognostic effect of *CYSTATIN C*

Survival analysis was performed using the sequence data of DNA and RNA, and clinical information that were obtained from TCGA database. Kaplan-Meier curves among (A and B) total breast adenocarcinoma patients. The patients were stratified into two groups according to (A) *p53* mutation, or (B) *CYSTATIN C* expression (above or below median) in tumors tissues. P-values were calculated by log-rank test.

Table 1. Sequences of DNA and RNA oligonucleotides

Quantitative real-time PCR	Forward	Reverse
Human EPSIN 3	GAGAAGCTAAAAACCAGCCAGT	CAGCAGAGCAGTGTGTGGA
Mouse Epsin 3	AAGGAGAGCCGGGACAGT	TGCCATTCTGCTTGCAACT
Mouse Epsin 3 for confirmation of knockout	CAAGACCAAAGAGCGAATGG	CTCCAGGTCTGAGGCATAGC
Human CYSTATIN C	ACTTCTTGGACGTGGAGCTG	GCACAGCGTAGATCTGGAAA
Mouse cystatin C	TGGTGAGAGCTCGTAAGCAG	CCCATCTCCACATCCAAAAA

Gene repoter assay	Forward	Reverse
Human *EPSIN 3* -p53BS	CCGCTCGAGCTTCCACCCACCTCCCTTAG	CCCAAGCTTGGATGATGTCAGGGGTAGGG
Human *EPSIN 3* -p53BS1mut	GGGTGTTGTCTGGGCCAGGTGGGGCT	CAGAATACCTCTTTCCCGAGCAGCTTGGC
Human *EPSIN 3* -p53BS2mut	GGATAGTTTTTCTTTGGAAGACCCTACCC	TGAATTACAGATTTTATGACTTTCTTGTC
mouse *Epsin 3* -mp53BS1	TCCAGCAAAACACACAGCTC	CCCCCTCTTTCTTTCACCTC
mouse *Epsin 3* -mp53BS2	CCGCTCGAGAGCCGGACAGAAAGACAGAA	CCCAAGCTTGCAAAAACTCCCCTTTCTCC
CYSTATIN C -p53BS	CCGCTCGAGCTAGGACTAGCGGCCTTCAC	CCCAAGCTTGTCTGTGTCACTGTTCGCTG
CYSTATIN C -p53BSmut	GACTCTTCCTCTATCAGCTGATGCAGAGT	AGGAATACTCCACCCCAGCAGGGACTCAG

ChIP assay	Forward	Reverse
Genomic fragment including p53BS2（*EPSIN 3*）	CCGTCCCAACAGCAAGAAG	CCCAAGCTTGGATGATGTCAGGGGTAGGG
Genomic fragment including p53BS (*CYSTATIN C*)	CTTCGTGCGTCCCAATTTTA	GTGTGTCTGTCCCTGGACTC

Expression vector	Forward	Reverse
EPSIN 3	AAAGAATTCTCTCCAGCCATGACGACCTC	TTTCTCGAGGAGGAAGGGGTTGGTGCCGG
EPSIN 1	AAAGAATTCGGCACCATGTCGACCTCGTC	TTTCTCGAGTAGGAGGAAGGGATTAGTG
CYSTATIN C	AAAGAATTCCCGACCATGGCCGGGCCCCT	TTTCTCGAGGGCGTCCTGACAGGTGGATT

Genotyping	Forward	Reverse
Mouse *p53*	GTTATGCATCCATACAGTACA	CCGCAGGATTTACAGACACC
Mouse *Epsin 3* wild-type	GGCAACCAGCTCTGTAAAACAGAGG	CCCTAGGTCACCCATTGTAAGAGGC
Mouse *Epsin 3* knockout	GGGATCTCATGCTGGAGTTCTTCG	CCCTAGGTCACCCATTGTAAGAGGC

siRNA oligonucleotides	Sense	Antisense
siEPN3-a	GCUCUAACAUUGCUGGACU	AGUCCAGCAAUGUUAGAGC
siEPN3-b	UCCAGACACUCAAGGACUU	AAGUCCUUGAGUGUCUGGA
siEPN3-c	GCACGUGUACAAGGCUCUA	UAGAGCCUUGUACACGUGC
siEPN3-d	CCUCGACCUUUGACCCAUU	AAUGGGUCAAAGGUCGAGG
siCystC-a	GGCACAAUGACCUUGUCGA	UCGACAAGGUCAUUGUGCC
siCystC-b	GCACAAUGACCUUGUCGAA	UUCGACAAGGUCAUUGUGC
siEGFP	GCAGCACGACUUCUUCAAGTT	CUUGAAGAAGUCGUGCUGCTT
sip53	GACUCCAGUGGUAAUCUACTT	AGUAGAUUACCACUGGAGUCTT

Table 2. Prognostic factors in Cox's proportional hazards model

Variables		Univariate		Multivariate	
		Hazard ratio (95% CI)	*P* -value	Hazard ratio (95% CI)	*P* -value
Expression of *cystatin C* (vs. above median)	Below median	1.656 (1.110 - 2.468)	0.0134	1.649 (1.054 -2.580)	0.0285
p53 status (vs. wild-type)	Mutant	1.560 (1.039 - 2.343)	0.0321	1.326 (0.838 - 2.098)	0.2277
Age (vs. <58*)	≥58	1.635 (1.094 - 2.445)	0.0166	1.877 (1.240 - 2.842)	0.0029
Pathological stage (vs. stage I)	II	1.283 (0.703 - 2.342)	0.4177	1.353 (0.739 - 2.476)	0.3275
	III	2.212 (1.163 - 4.206)	0.0155	2.384 (1.252 - 4.540)	0.0082
	IV	4.233 (1.823 - 9.825)	0.0008	4.008 (1.723 - 9.321)	0.0013

* Median age; CI, confidence interval

Acknowledgements

I would like to acknowledge scientific guidance and support of Professor Koichi Matsuda, whose enthusiasm and scientific endeavor have been a constant source of encouragement during my three years of doctorate course. He provided me strategic and productive supports essential to complete this project.

I would like to show my appreciation to all of members in our laboratory for the mentorship and experimental advice throughout the research activity.

Finally, I would like to appreciate my wife and sons for their encouragement of me during my study period.